Correspondence to:

K. Sauer,
sauer.ka@gmail.com

The copyright line for this article was changed on 6 OCT 2022 after original online publication.

Multi-Ion Oscillitons—Origin of Coherent Magnetospheric EMIC Waves

Konrad Sauer[2] and **Eduard Dubinin[1]**

[1]Max-Planck Institute of Solar System Research, Göttingen, Germany, [2]Retired from Max-Planck Institute of Solar System Research, Göttingen, Germany

Abstract The recent spacecraft observations by MMS and Van Allen Probes associated with electromagnetic ion cyclotron (EMIC) waves in the Earth magnetosphere emphasize the important role of multi-ion plasma composition for generation and characteristics of these emissions. We show that main properties of the coherent EMIC waves can be explained with the concept of "multi-ion oscillitons" (Sauer et al., 2001, https://doi.org/10.1029/2001GL013047). In a plasma with two types of ions of different masses (e.g., protons and oxygen ions), oscillitons arise from the exchange of momentum and energy between the two ion components, with the electromagnetic field acting as a mediator. At frequencies near cross-over frequencies of different wave modes in the multi-ion plasma the nonlinear resonance which strongly amplifies the seed unstable mode can be excited. A small phase difference in oscillations of different ion species leads to a nonlinear wave beating and generation of wave packets. The "resonance" frequency is characterized by a local maximum of the phase velocity and the coincidence of phase and group velocity. It is suggested that the oscillitons are triggered by the instability due to the proton temperature anisotropy and may survive outside the source region for long distances. The generation of coherent waves by oscillitons is of a general nature and may contribute to understand the manifold of phenomena in other space plasma environments in which the dynamics of minor ion admixtures cannot be neglected. The concept of oscillitons can also be applied to the momentum exchange between particle groups of the same mass, but different temperature.

Plain Language Summary The mode splitting of electromagnetic waves at oblique propagation in plasmas with multiple ion species leads to the creation of gap regions in omega-k space. In these "forbidden regions" spatially growing waves exist whose nonlinear state represents a new type of solitons. These so-called oscillitons, first described by Sauer et al. (2001, https://doi.org/10.1029/2001GL013047), arise from momentum and energy exchange between two or more ion components, with the electromagnetic field acting as a mediator. We suggest that multi-ion oscillitons are the origin of the ion cyclotron electromagnetic waves (EMIC) in the magnetosphere, which have been known for a long time. Valuable insights have recently been gained through improved diagnostics on the satellites MMS and Van Allen Probes.

1. Introduction

Over the last years significant progress has been made in obtaining high-time and spatial resolution of waves in space plasmas. The interesting class of the observed wave emissions is coherent wave structures in the form of wave packets. Examples are near monochromatic packets of right-hand circularly polarized waves (lion roars) (Baumjohann et al., 1999; Dubinin et al., 2007; Y. Zhang et al., 1998), large amplitude quasi-monochromatic ULF waves in the ion foreshock (Fazakerley et al., 1995; Fuselier et al., 1986), narrow-band chorus emissions (Tsurutani & Smith, 1974; Tsurutani et al., 2020). Often such structures are observed in plasmas which contain different ion populations. It was suggested that these waves might represent a new class of solitary waves containing solitons with an embedded smaller scale oscillating core and therefore were called oscillitons (Dubinin et al., 2002, 2004; Dubinin, Sauer, & Mckenzie, 2003, Dubinin, Sauer, Mckenzie, & Chanteur, 2003a, 2003b; Sauer & Sydora, 2011; Sauer et al., 2001, 2002, 2003). These nonlinear structures are produced by a nonlinear resonance driven by the momentum exchange between the protons and electrons in whistler modes or between an ion beam and the main plasma or between the different ion populations in multi-ion plasmas, or even between two proton populations with different temperatures. In all such cases the momentum exchange is mediated by the Maxwell magnetic stresses. It occurs that phases of wave oscillations of the interplaying particles are slightly different that results in a wave beating and creation of wave packets (Dubinin, Sauer, & Mckenzie, 2003). It is interesting to note that the existence of such nonlinear structures can be predicted from a dispersion analysis even

without the exact solutions. The favorable conditions are realized when the phase velocity exhibits a maximum (inflection point in ω-k space). For example, for whistlers in a cold plasma it happens at $\omega_{He}/2$. In multi-ion plasma it happens near cross-over frequencies of different wave modes. The feature of this frequency at which the phase and the group velocities are matched is that the wave packets will be bunched up there. Different types of plasma instabilities driven either by a beam or by a temperature anisotropy can excite a broad range of emissions. The mode at which the nonlinear resonance might be excited is selected from the ensemble of the linearly unstable waves and amplified as the system resonates at this frequency.

Electromagnetic ion cyclotron (EMIC) waves bring us another example of coherent wave structures. The improved technology of recent spacecraft missions associated also with multi-point measurements has achieved a wealth of new data about these waves. The new observations emphasize an important role of multi-ion plasma composition for generation and characteristics of EMIC waves. Multi-ion composition is a common feature for space plasmas. Even a small admixture of a second ion component to a proton-electron plasma can significantly change wave characteristics and plasma flows. The presence of a tenuous He^{++} component in solar wind modifies the dispersion of plasma waves and leads to a change of polarization near the cross-over frequency. Such effects were recently observed by the Solar Orbiter (Khotyaintsev et al., 2021). A change in dispersion may result in appearance of a new class of nonlinear waves in the plasma of protons and α-particles (Dubinin, Sauer, Mckenzie, & Chanteur, 2003a, 2003b). Left-handed MHD waves arising near the cross-over frequency may also be an important agent in the coronal heating of the solar wind (Li & Habbal, 2001). Inclusion of alpha-particles into a proton-electron plasma can also reduce the growth rate of the proton cyclotron instability and control a dominance of ion cyclotron or mirror waves (Gary et al., 1994). Multi-ion component plasmas are also typical for comets where we observe a rich variety of waves and coherent structures (Tsurutani, 1991). Multi-ion origin of plasma is also manifested near Venus and Mars (Nagy et al., 2004) with extended exospheres, or Jupiter (T. K. Kim et al., 2020) and Saturn (Thomsen et al., 2010) and their moons.

In this paper, we show that diverse phenomena of coherent magnetospheric EMIC waves can be explained with the concept of "multi-ion oscillitons." The theoretical background of oscillitons in the frequency range of EMIC waves is formed by the multi-ion Hall-MHD equations which are derived from the multi-fluid equations by replacing the electric field via the assumption of mass-less electrons and by using charge neutrality. In general, a three-ion plasma of protons, single charged helium and oxygen is considered. By solving the dispersion relation of cold ions one gets a first survey about the ω-k position of the cross-over frequencies together with the k-variation of the wave polarization as function of the abundance ratios and the wave propagation angle. In the next step, the linear characteristics of stationary waves $k = k(U)$, that is the wave number as function of the velocity U of the moving frame in which the wave is stationary, are determined. They represent a useful pre-information in solving the full nonlinear, stationary Hall-MHD equations to get the spatial profiles of oscillitons. Several examples of the calculated wave packets are given. In addition it is shown that oscillitons also exist in multi-ion plasmas where two heavy-ion populations of the same mass but with different temperatures or streaming velocities are present. This leads to oscilliton frequencies very close to heavy-ion cyclotron frequency, in contrast to the more common case where the cross-over frequency is above the cyclotron frequency of the heavy ion population. We also compare the theoretical results with the properties of observed EMIC events in space. Since EMIC waves are more extensively studied near the Earth we make a comparison with recent observations in the Earth magnetosphere. It concerns the frequency, the wave polarization and possible plasma parameters which can be derived from the theoretical model. The influence of kinetic damping due to finite electron and ion temperatures is discussed, too.

2. Theoretical Background of Oscillitons

According to the magnetospheric conditions, we consider a space plasma which consisting of electrons and three ion populations, protons single-ionized helium and oxygen, here denoted by the indices p for protons, h for He^+, and i for O^+, respectively. With the proton density n_{po} as reference, a standard composition of 10% helium ($n_{ho}/n_{po} = 0.1$) and 5% oxygen ($n_{io}/n_{po} = 0.05$) is assumed. The starting point are the multi-fluid equations which have been used in earlier papers on non-linear stationary waves (Sauer et al., 2001, 2002, 2003, 2011; Dubinin et al., 2002; Dubinin, Sauer, & Mckenzie, 2003; Dubinin, Sauer, Mckenzie, & Chanteur, 2003a, 2003b; McKenzie et al., 2004). They follow in a straightforward way from the usual multi-ion equations by eliminating the electric field by the following assumptions which are relevant to the low-frequency processes under consideration:

(a) massless electrons and (b) charge neutrality, that is, $n_e = n_p + n_h + n_i$. This so-called Hall-MHD model is described for example, by Huba (2003) in detail and has been applied for many purposes in space physics, as for modeling the solar wind interaction with non-magnetized bodies, for example, Sauer et al. (1994), Nagy et al. (2004), and Rubin et al. (2014). A summary of these equations can be found in Appendix A.

2.1. Multi-Ion Dispersion Theory

In order to analyze the dispersion characteristics of low-frequency waves in multi-ion plasmas, the linearized version of the Hall-MHD equations are solved for plane waves in the common way. The applied tensor formalism is similar as described before by Sauer and Sydora (2010). After Fourier transform (all variables vary as $\sim\exp(-i(\omega\text{-}\mathbf{k}\cdot\mathbf{x})))$, the fluid and Maxwell equations are written in tensor form which by means of matrix operations of *Mathematica* (Wolfram, 1988) finally leads to the equation

$$\mathbf{M}(\omega, \mathbf{k}) \cdot \mathbf{E}(\omega, \mathbf{k}) = \mathbf{0} \tag{1}$$

where $\mathbf{M}$ is the multi-ion dispersion tensor as a function of ω and $\mathbf{k}$ which contains the undisturbed plasma parameters (density, velocity, temperature, mass, charge) of the ion populations in addition to the propagation angle θ with respect to the magnetic field which was taken in z-direction. From there, one gets the dispersion relation

$$D = \text{Determinant}[\mathbf{M}] = 0. \tag{2}$$

It represents a polynomial (with real coefficients) of nth order in ω as function of k where n depends upon how many particle populations are taken and whether they are considered as cold or warm or a beam population is present. Further, using the matrix relation (Equation 1), the polarization of the multi-ion waves can easily be calculated. From the three equations for the electric field components E_x, E_y, and E_z the polarization (ε) is obtained as the ratio $\varepsilon = i\, E_y/E_z$ by simple algebra. Similar dispersion analysis of cold multi-ion plasmas has been done long before, for example, by Smith and Brice (1964), Rauch and Roux (1982), and Thompson et al. (1995). Our focus of dispersion analysis is mainly directed on the coupling between different wave modes which occurs if the waves propagate oblique to the magnetic field.

In Figure 1, solutions of the dispersion relation (Equation 2) are shown for two cases. The three panels of Figure 1a belong to a multi-ion plasma consisting of cold protons, single-ionized helium and oxygen with an abundance ratio (with respect to the proton density) of $N_{He}^+ = 10\%$ and $N_O^+ = 5\%$. The propagation angle is $\theta = 15°$. The essential effect of interest is the mode splitting between the two kinds of waves, the originally right-hand polarized R-mode and the originally left-hand polarized L-modes which arise due to the heavy-ion abundance. Whereas at parallel propagation these modes cross each other without any effect, frequency gaps arise at the cross-over points (marked by the red and blue dashed circles) if the waves propagate oblique to the magnetic field. Characteristic frequencies which are related to the heavy-ion abundances and needed for later discussion are the two cut-off frequencies (at $k = 0$), approximately given by $\omega_{cut1} \sim \Omega_p(n_O^+/n_p + m_p/m_O^+) = 0.11$ and $\omega_{cut2} \sim \Omega_p(n_{He}^+/n_p + m_p/m_{He}^+) = 0.35$ (Ω_p: proton cyclotron frequency), and the two cross-over frequencies which are located above their related cut-off frequencies. As a remarkable feature, the phase velocity shown in middle panel (a) gets a maximum (minimum) at the mode crossing points. As one could imagine and can clearly be seen in the bottom panel, a change of polarization at the cross-over frequencies takes place. For example, the dotted curve which is R-polarized at small wave numbers k changes to linear polarization at the point of maximum phase velocity (marked by the blue dashed circle) and goes with increasing k over to left-hand polarization. A similar behavior takes place for larger wave numbers at the second cross-over point (red dashed circle) at ($\omega/\Omega_p \sim 0.4$, $kc/\omega_p \sim 0.4$) which is associated with the He$^+$ abundance. Observation of EMIC waves with linear polarization is partly explained in literature via mode conversion (Jun et al., 2021; Young et al., 1981) when the propagating waves approaches the cross-over point. We come back to this in the discussion.

The second example of multi-ion dispersion analysis, shown in the three panels of Figure 1c, concerns a case where mode splitting appears due to the existence of two ion populations of the same mass, but with different temperatures. Here, cold and hot proton populations are considered. As we will discuss later, this situation creates requirements of EMIC wave generation very close to the proton cyclotron frequency, or more general, close to the cyclotron frequency of two-temperature heavy ions under consideration. As in Figure 1a from top to bottom the frequency, the phase velocity and polarization are shown. As seen, the mode splitting effects are similar as for
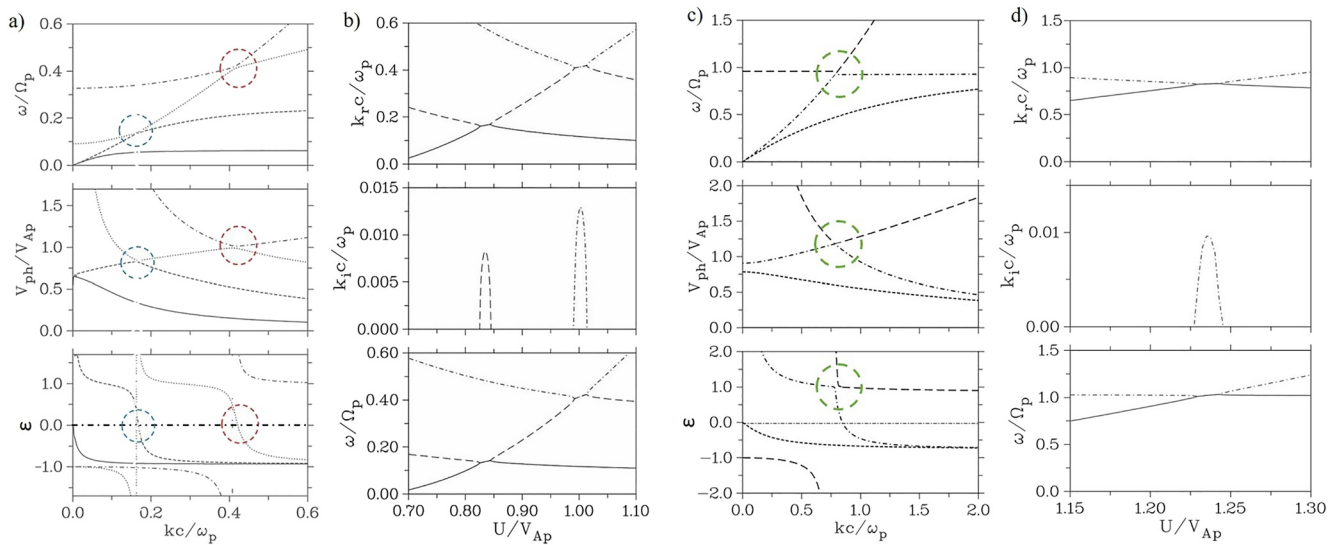
Figure 1. Multi-ion dispersion theory and linear stationary waves, fluid approach. (a) The left three panels belong to the cold plasma consisting of electrons, protons, He$^+$ and O$^+$ ions. The heavy-ion densities normalized to the proton density are $N_{He+} = 10\%$ and $N_{O}^+ = 5\%$, respectively. The propagation angle is $\theta = 15°$. From top to bottom: the (normalized) frequency ω/Ω_p, the (normalized) parallel phase velocity V_{ph}/V_{Ap} (V_{Ap}: proton Alfven velocity) and the polarization ε (epsilon) versus the (normalized) wave number kc/ω_p (ω_p: proton plasma frequency). The dashed blue and red circles mark the cross-over points in the H$^+$ and He$^+$ bands, respectively. (b) Linear stationary multi-ion waves $k = k(U)$ resulting from the dispersion relation of the propagating waves in (a) by the replacement $\omega \rightarrow k \cdot U$ where U is the velocity of the moving frame. From top to bottom: real and imaginary part (spatial growth rate) of the wave number kc/ω_p and the "oscilliton frequency" ω/Ω_p versus U/V_{Ap}. As seen in the middle panel, growing stationary waves occur at the mode-crossing points. (c) The same format as in (a) showing the dispersion $\omega = \omega(k)$ of a two-temperature plasma of cold and warm protons (relative density $N_H^+ = 25\%$, $\beta_H^+ = 0.25$); $\theta = 25°$. The cross-over points are marked by green dashed circles. (d) Stationary waves $k = k(u)$ in the two-temperature plasma of Figure 1c. Maximum spatial growth rate (middle panel) appears at the "oscilliton frequency" $\omega = k_r \cdot U$ (bottom panel) very close to the proton cyclotron frequency Ω_p.

EMIC waves in the proton plasma with heavy-ion abundances. At the cross-over (ω, k) point, marked by the green dashed circle, the phase velocity has a maximum (minimum) and changes the polarization there from right- to left-hand polarization (and vice-a versa).

2.2. Linear Stationary Waves

A next step in accordance with the approach to oscillitons in the original paper by Sauer et al. (2001) consists in the proof of linear stationary waves in the gap areas around the cross-over points. For this purpose the frequency in the dispersion relation 2.2 is replaced by $\mathbf{k} \cdot \mathbf{U}$ where U is the velocity of the moving frame. With $\omega = \mathbf{k} \cdot \mathbf{U}$, Equation 2 is transformed in a polynomial in k as function of the "oscilliton velocity" U. Solutions of the resulting dispersion relation of stationary waves $D(\mathbf{k} \cdot \mathbf{U}, k) = 0$ are shown in Figures 1b and 1d. By comparison with the related plots of Figures 1a and 1b one can clearly see that growing stationary waves with $k_i > 0$ (k_i: imaginary part of k) occur just there, where "forbidden" areas in the (ω, k) space owing to mode splitting arise. According to Figure 1b, due to the presence of two heavy ion populations (helium and oxygen), one gets two ranges of "oscilliton" velocities with the related frequencies $\omega = \mathbf{k} \cdot \mathbf{U}$ and (real) wave numbers. For the selected abundance ratios of 5% O$^+$ and 10% He$^+$ and a propagation angle of $\theta = 15°$, the associated "oscilliton" frequencies are $\omega \lesssim 0.2\Omega_p$ and $\omega \lesssim 0.45\Omega_p$, respectively. How these frequencies vary with the propagation angle will subsequently be discussed. Figure 1d belongs to the plasma with both a cold and hot proton population. As an essential signature one has to note that for this kind of plasma a growing stationary wave with a frequency close to the proton cyclotron frequency arises. In plasmas with heavy-ion admixtures, on the other hand, a comparable approaching to this frequency cannot be achieved by reasonable abundance ratios.

From the two examples which have been described in Figure 1 it is evident that the analysis of the stationary waves in multi-ion plasmas represents a simple tool in order to get useful predictions for further studies. So, the growth rate of stationary waves can easily be used to determine the associated "oscilliton frequency" in dependence of main parameters, as propagation angle or the abundance ratio of heavy-ions. For a given propagation angle θ, for example, the maximum growth rate is determined versus the abundance ratio (heavy-ion density/proton
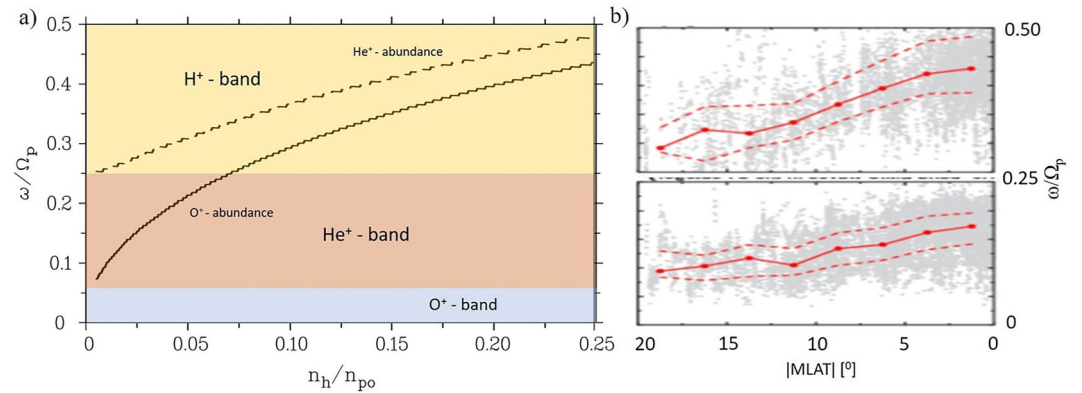
Figure 2. (a) "Osciliton frequency" versus the He^+ (dashed curve) and O^+ abundance ratio (solid curve), respectively, for a fixed propagation angle of $\theta = 15°$. The dependence has been determined from the maximum growth rate of stationary waves $k = k(U)$, whereby only one heavy ion population was considered as an addition to the proton plasma. That means, the index "h" stands for "He^+" and "O^+" separately. (b) Statistical Van Allen Probe measurements of the normalized frequency of EMIC waves in the H^+ (upper panel) and He^+ band (lower panel) versus |MLAT|, adapted from Jun et al. (2019).

density) of O^+ and He^+ ions, respectively. From the "osciliton velocity" U at maximum spatial growth and the associated (real) wave number kr, one then obtains the "osciliton frequency" $\omega = k_r \cdot U$, which according to our general philosophy is almost identical to the corresponding cross-over frequency. Such a dependency is shown in Figure 2 for a fixed propagation angle of $\theta = 15°$, where in the range of small angles ($\theta \lesssim 30°$) there are only relatively small shifts in both curves. It is noteworthy that due to He^+ even with moderate admixture (<25%), the "osciliton frequency" remains below $0.5\ \Omega_p$. Comparing Figures 1 and 2, we note that in the plasma with only He^+ admixture the osciliton frequency occurs somewhat less than in the plasma with both additional ion species (He^+ and O^+). With O^+, on the other hand, a frequency shift from the He^+ band to the H^+ band can already take place with an addition of less than 10%. As we will discuss, this dependency is directly related to statistical results from satellite measurements, see for example, Jun et al. (2021).

In Figure 3, the spatial growth rate $k_i c/\omega_p$ and the related frequency ω/Ω_p of EMIC oscilitons in plasmas with He^+ and O+ abundance, respectively, versus the propagation angle θ are shown. For He^+, in panels (a and b) results for the abundance ratios 0.01 (dashed curves), 0.05 (dotted) and 0.10 (solid) are presented. Whereas the spatial
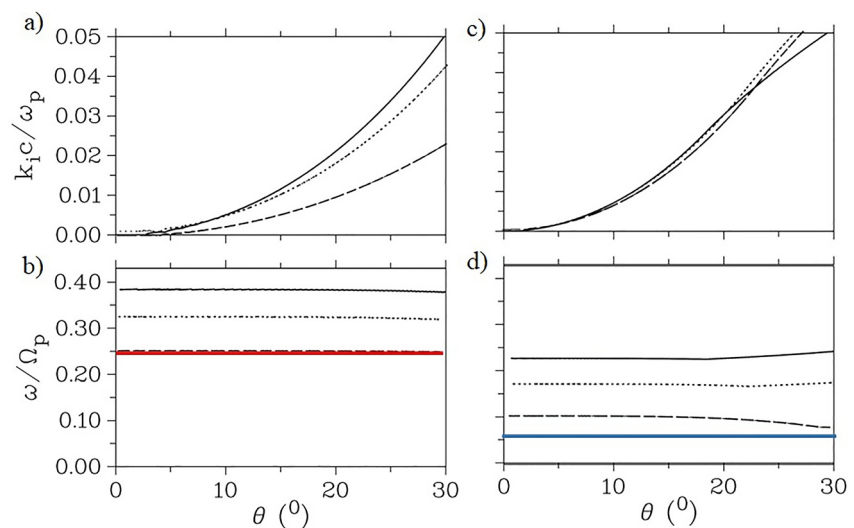
Figure 3. (a and c) Spatial growth rate and (b and d) related frequency of electromagnetic ion cyclotron oscilitons for three abundance ratios of He^+ and O^+ respectively, versus the propagation angle θ. The He^+ abundance ratio in (a and b) is 0.01 (dashed), 0.05 (dotted), and 0.10 (solid). The abundance ratio of O^+ in (c and d) is 0.005 (dashed), 0.025 (dotted), and 0.05 (solid). The solid red line in (a) and blue line in (d) mark the He^+ and O^+ cyclotron frequency, respectively.

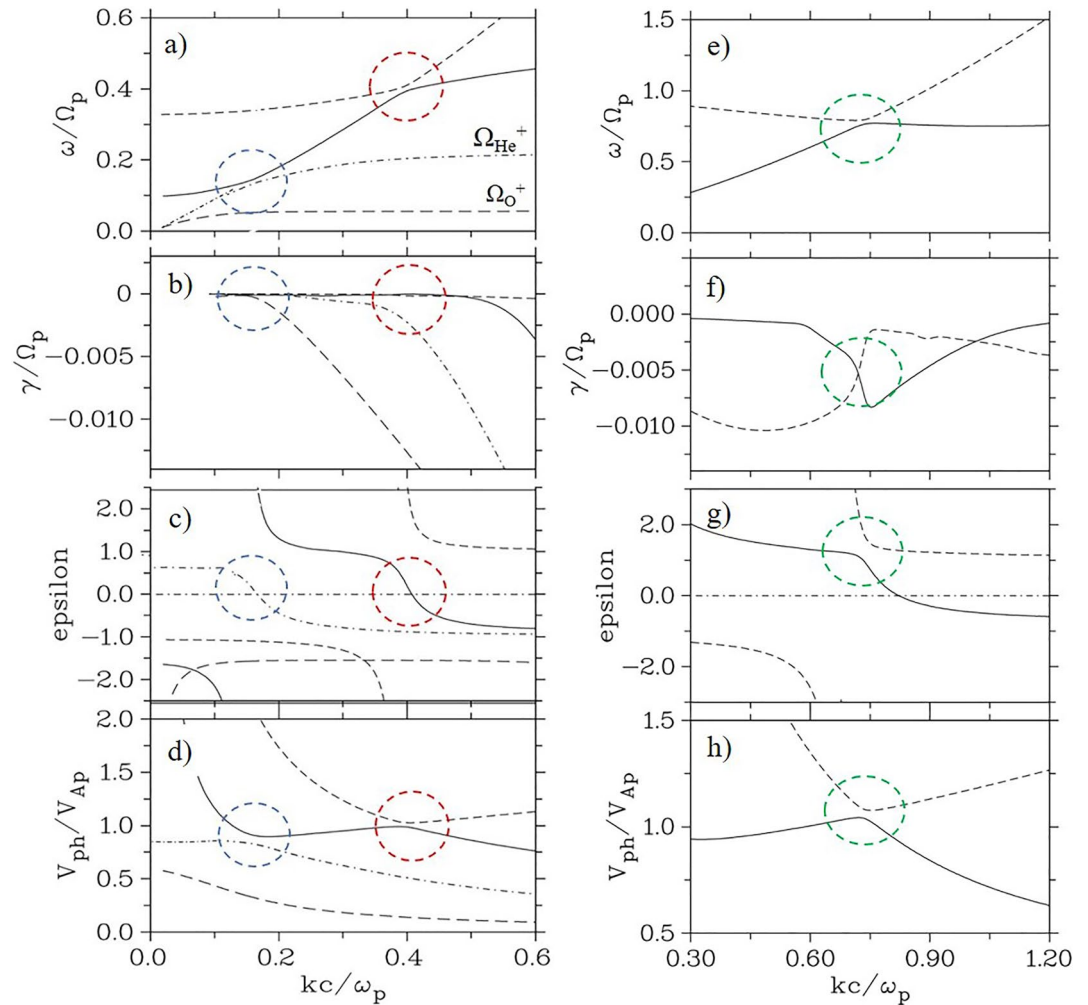**Figure 4.** Similar format as in Figure 1, however, instead of fluid theory the Vlasov dispersion relation including kinetic damping by finite electron and ion temperatures has been used. The damping rate γ/Ω_p is added in the second raw, panels (b and f). For the multi-ion case (left panels) the temperatures of the ions (H^+, He^+, and O^+) are given by $\beta_{H^+} = 0.15$ and $\beta_{He^+} = \beta_{O^+} = 0.01$. For the electrons $\beta_e = 0.2$ was used. The right panels belong to two-temperature plasma of cold ($\beta_{H^+} = 0.001$) and warm protons (relative density $N_{H^+} = 25\%$, $\beta_{H^+} = 0.25$); $\theta = 25°$.

growth rate k_i increases with increasing propagation angle, the oscilliton frequency remains nearly constant in the interval up to $\theta = 30°$. It varies with the abundance ratio from slightly above the He^+ cyclotron frequency ($\omega/\Omega_p = 0.25$) up to about 0.4 Ω_p (see also Figure 2). In panel (c) the growth rate is shown versus the propagation angle θ for O^+ abundance ratios of 0.005 (dashed line), 0.025 (dotted) and 0.05 (solid). Remarkably, there is only a weak dependence on the heavy ion density. The frequency in turn increases from $\omega/\Omega_p \sim 0.1$ to 0.25 with a slight decrease if θ increases.

2.3. Kinetic Dispersion Analysis (Vlasov Approach)

In order to analyze to what extent the multi-fluid theory results shown in Figures 1a and 1c are influenced by kinetic damping effects, our own code to solve the kinetic dispersion relation was used. This code written on the formalism of Stix (1992) has successfully applied for different purposes, for example, Sauer and Sydora (2011). Hereby, the knowledge of the fluid results made it easier to find the corresponding solutions of the Vlasov description. Results for the same parameters as in Figure 1 with respect to the abundance ratios and propagation angles, supplemented by the plasma temperatures of electrons and ions via the related plasma betas β_i (i: e, H^+, He^+, O^+) are shown Figure 4. Looking first to the left two panels for the multi-ion dispersion at presence of protons, helium and oxygen ions, the good agreement between both approaches with respect to the real part of

frequency in (a), the polarization in (c) and the phase velocity in (d) is visible. As additional information one gets the kinetic damping in panel (b). As a remarkable effect one has to note the onset of significant damping of the left-hand polarized (cyclotron) modes after their crossing of the weakly damped right-hand mode. The right panels (e–h) show the dispersion behavior in the vicinity of the proton cyclotron frequency for the case that the proton plasma consists of a cold ($\beta_c = 0.001$) and hot population ($\beta_h = 0.02$) whose density is 25% of the cold one. Essential effects are again the pronounced mode splitting between the both modes of different polarization and the associated formation of an inflection point where phase and group velocity coincide.

2.4. Spatial Oscilliton Profiles

The final step to oscillitons is the calculation of their spatial profiles by solving the stationary nonlinear fluid equations. The procedure of deriving the governing system of ordinary differential equations is detailed described in earlier papers by Sauer et al. (2001, 2002), Sauer and Sydora (2011), Sauer and Dubinin (2003), Dubinin et al. (2002, 2004), Dubinin, Sauer, Mckenzie, and Chanteur (2003a, 2003b), Dubinin, Sauer, and Mckenzie (2003), and McKenzie et al. (2004) and, therefore, only few explanations are given here. Starting point are the Hall-MHD equations as already explained in Section 2.1. In the one-dimensional model the *x*-direction is determined by the direction of the wave propagation. The *y*- and *z*-axes complete the orthogonal system, with the magnetic field lying in the *x-z* plane and forming the angle θ with the *x*-axis. The search for stationary waves means switching to the reference system, in which there is no time dependence. That is, $\partial/\partial t$ is replaced by $-U \, d/dx$, where U stands for the so-called oscilliton velocity. Thus, the complete system of nonlinear equations in *x* and *t* is converted into a system of ordinary differential equations. Using in addition the conservation of mass flux and transverse momentum, for a plasma with three ion species (protons, helium and oxygen ions), finally nine equations are required to determine the relevant quantities, that is, density, velocity of ions and the magnetic field. Essential parameters are the abundance ratios of the heavy ions and the temperatures of electrons and ions, expressed by their plasma betas β_i. They together with the propagation angle θ determine the range of "oscilliton velocities" U in which, according to the linear theory in Section 2.2, spatially increasing solutions with the corresponding spatial growth rates occur. (For the simple case of the cold two-ion plasma, the equations to be solved are given explicitly in Appendix B.)

The following normalizations are used below: The densities relate to the proton density n_{po}, the velocities are normalized with the proton Alfven speed V_{Ap}. The magnetic field disturbances refer to the undisturbed magnetic field B_0 and finally the electric fields are normalized with $E_0 = V_{Ap} B_0$. As a first example, the spatial profiles are determined for the case that three ion populations take part at the momentum coupling between magnetized ions and the electromagnetic field. As before, a plasma of protons with a proportion of 10% helium (He$^+$) and 5% oxygen ions (O$^+$) is assumed. According to the descriptions in the previous sections (Figures 1a and 1b), such a three-ion plasma has two cross-over frequencies and thus two propagation velocities U at which oscillitons are to be expected. In the context of our fluid model, these are determined by the abundance ratios and the propagation angle. In the following we choose $\theta = 15°$ and determine the spatial profiles of the oscilliton in the He$^+$ band due to the O$^+$ abundance, which according to Figure 1b exists at M $\sim$ U/V_{Ap} $\sim$ 0.83 with kc/ω_p $\sim$ 0.22 and thus $\omega/\Omega_p = 0.18$. The numerical integration of the differential equations describing the spatial oscilliton profiles results in the plots of Figures 5a and 5b. In Figure 5a, the hodograms of the transverse velocities and of the transverse magnetic field are shown, whereby the index "h" stands for He$^+$ and "i" for "O$^+$." The corresponding spatial variation of the z-component of the four quantities is pictured below in Figure 5b. From the hodograms one can see the tendency toward linear polarization and the close correlation between the rotating motion of the ions and the behavior of the magnetic field. Further, it can be seen that there is a 90° phase shift between the rotation of O$^+$ and He$^+$.

Of a particular interest is the occurrence of EMIC waves in the immediate vicinity of the cyclotron frequency of an ion species present in the plasma. For example, Teng et al. (2019) describe the generation and characteristics of emission at the proton cyclotron frequency. These particular EMIC events are interpreted as oscillitons which are based on the presence of two populations of the same mass but with different temperatures or drifts. As analyzed in Figures 1c and 1d, mode coupling takes place here between the two components and leads ultimately to the possibility of stationary growing waves. A corresponding example is shown in the panels of Figures 5c and 5d, where the interaction between two proton populations of different temperature generates an oscilliton very close to the proton cyclotron frequency. In the present case it is assumed that the plasma consists of cold protons
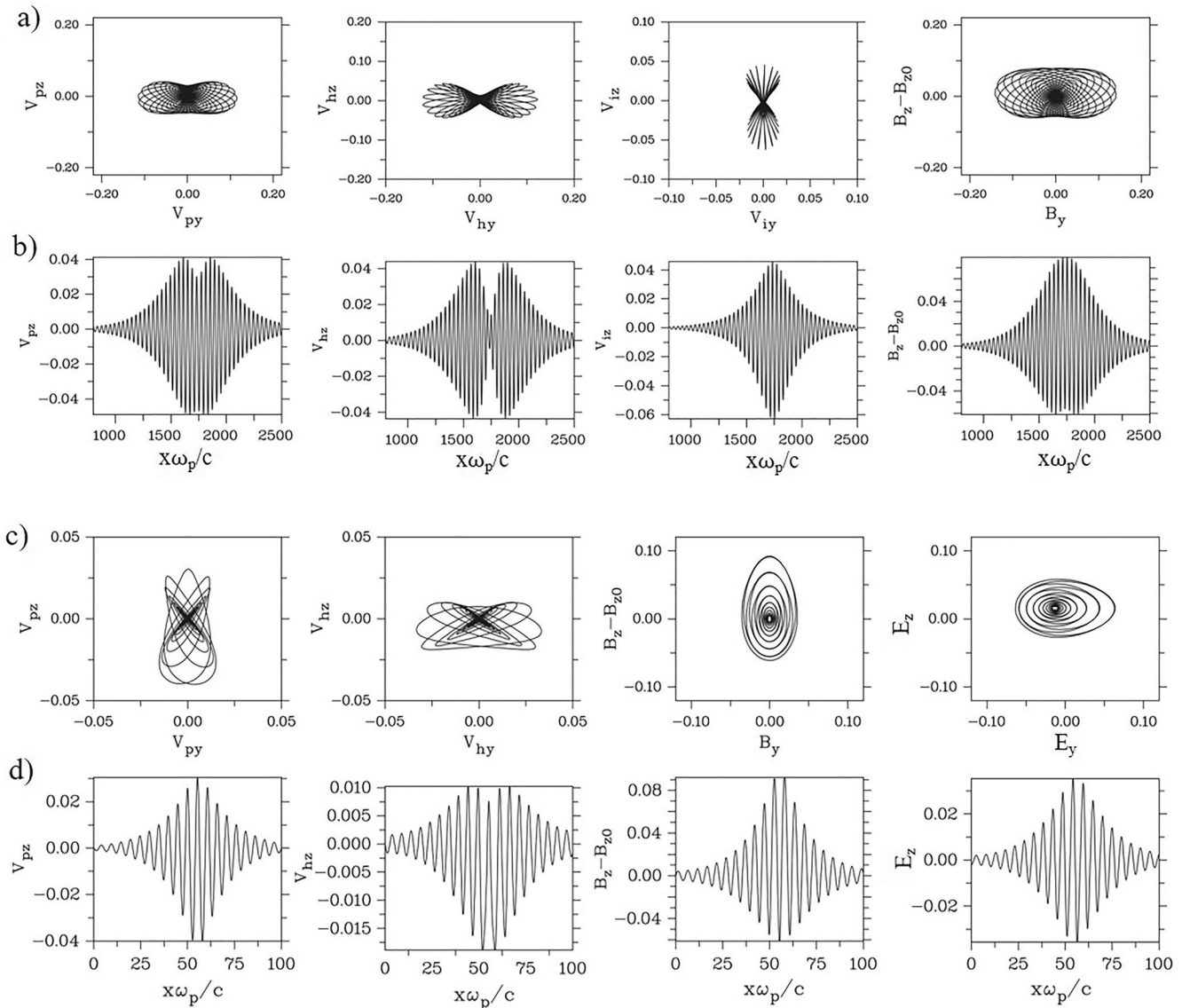
Figure 5. Hodograms and spatial profiles of oscillitons: (a and b) Multi-ion plasma consisting of three (cold) ion populations: protons, He$^+$-ions (10% of the proton density) and O$^+$-ions (5% of the proton density). The oscilliton moves with the velocity $M = 0.83$ which corresponds to a frequency of $\omega/\Omega_p = 0.18$. The propagation angle is $\theta = 15°$. Panel (a) shows the hodograms of the transverse velocities (indices: p for protons, h for He$^+$ ions and i for O$^+$ ions) and of the transverse magnetic field. The corresponding spatial oscilliton profiles are shown in panel (b). Panels (c and d) belong to a two-temperature proton plasma which consists of a cold (index p) and warm population (index h) of the same density with $\beta_h = 0.2$. The propagation angle is $\theta = 60°$. The oscilliton velocity is $U = 0.83\,V_{Ap}$. The resulting oscilliton frequency is very close to Ω_p. In the last panels (c and d) the hodogram of the electric field (E_z over E_y) and the spatial variation of E_z, respectively, are shown in addition.

(index p) with the same admixture of warm protons (index h) with $\beta_h = 0.2$. For $\theta = 60°$, the oscilliton velocity is $M = 0.83$ and with kc/$\omega_e = 1.24$ one gets an "oscilliton frequency" of $\omega/\Omega_p \sim 1$. As can be seen from the first two hodograms in Figure 5c, the two proton groups ("p" for the cold population, "h" for the hot one) perform very different gyrating motions, which finally, as a result of the self-consistent interaction, causes the particular polarization of the magnetic field, plotted in the third hodogram. What the different particle gyrations look like in detail depends on the respective parameters of the proton groups. Remarkable is the significant variation of the density of cold ions (not shown here), which reaches almost 10%, which is also similarly reflected in the amplitude variation of the magnetic field. In the fourth panels of Figure 5c the hodogram of the electric field is shown, whereby E_y, E_z are related to B_y, B_z by $E_y = M \cdot (B_z - B_{z0})$ and $E_z = -M \cdot B_y$. In the four panels of Figure 5d, finally, the spatial profiles of the z-component of the proton velocities (V_{pz} and V_{hz}), of the magnetic field ($B_z - B_{z0}$) and
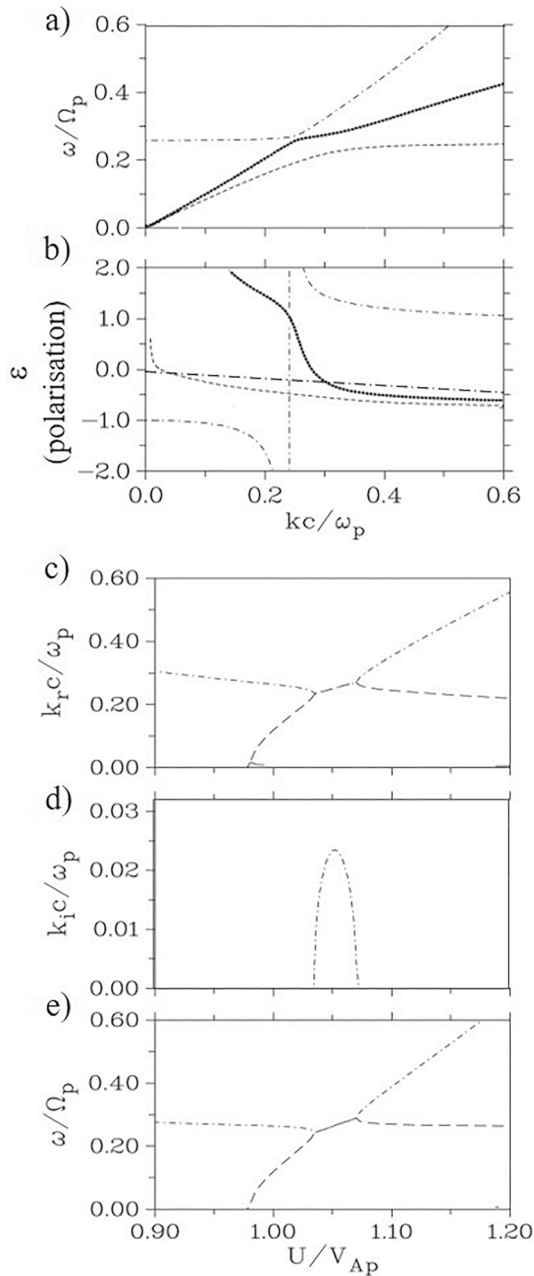
Figure 6. (a and b) Dispersion of electromagnetic ion cyclotron waves and of (c–e) stationary waves in a proton-He$^+$ plasma; the same format as in Figure 1. In contrast to earlier parameters, the abundance ratio of He$^+$ is small ($n_{He^+}/n_0 = 0.01$) and the propagation angle is $\theta = 30°$. Note the right-hand polarization of the original Alfven mode at large wave numbers (solid line) at the mode crossing point reaching kc/$\omega_e \sim 0.25$. Panels (c–e) show the related dispersion of stationary waves, $k = k(U)$. Maximum growth rate of $k_i c/\omega_p \sim 0.02$ occurs at $U/V_{Ap} = 1.05$ which involves with kc/$\omega_e \sim 0.25$ an oscilliton frequency of $\omega \gtrsim 0.25 \, \Omega_p$, s.a. Figure 3b.

of the electric field (E_z) are pictured. As will be shown later, the mutual drift of two particle populations of the same mass and temperature can lead to similar effects.

2.5. Example of Right-Hand Polarized p-He$^+$ Oscilliton

One characteristic feature of the multi-ion oscillitons so far considered in Section 2.3, see Figure 5, was their left-hand polarization. The question was are there conditions under which right-hand polarized oscillitons exist. One tendency which can be gained already from the linear theory of multi-ion waves is that the polarization at the cross-over frequency is shifted more and more to $\varepsilon > 0$ (right-hand polarization) if the propagation angle increases. Since, in turn, multi-ion oscillitons at pronounced oblique propagation can exist only in case of small heavy-ion abundance, our search for right-hand polarized oscillitons was done in this direction. Under this point of view, a proton plasma containing only 1% He$^+$ admixture (instead of 10% before) is considered in the following investigations, with a propagation angle of $\theta = 30°$ being selected. In Figure 6 corresponding results of the linear theory are shown. Panels (a and b) present the frequency ω/Ω_p and the polarization ε versus kc/ω_p, respectively. The outcome of linear stationary theory is shown in the panels (c–e) in the same format as in Figures 1b and 1d. As seen in Figure 6d, maximum spatial growth of $k_i c/\omega_p \sim 0.02$ occurs at the oscilliton velocity of $U/V_{Ap} \sim 1.05$. The related oscilliton frequency (Figure 6e) is $\omega/\Omega_p \sim 0.27$.

The spatial oscilliton profiles are obtained by solving the system of ordinary differential equations given in Appendix B. The corresponding results are shown in Figure 7, where the right-hand polarization of the EMIC oscilliton is to be emphasized. The hodograms of the transverse proton (V_{py}, V_{pz}) and He$^+$ velocities (V_{hy}, V_{hz}) in panels (a and b), respectively, indicate that the gyration velocities of the He$^+$ ions are larger than those of the protons. This is an effect of the low He$^+$ density of 1%. In the panels (d–i), the spatial profiles of V_{pz}, V_{hz}, V_{py}, V_{hy}, B_z-B_{z0}, and B_y are shown. From there, the phase relations between all these quantities can be read.

2.6. Harmonic Generation

Stimulated by the observation of the harmonics of the EMIC waves, for example, Usanova et al. (2016), the question has become topical as to whether and in what way the stationary, non-linear structures of oscillitons can be a source of higher harmonics. Surprisingly, the Fourier analysis of the spatial profiles as shown in Figure 4 has produced results that are apparently directly related to the characteristic features of observed harmonics. It turned out that the properties of the harmonics generated by the oscilliton depend crucially on which wave modes are involved in its formation and in which (ω, k) space this occurs. Guided by the observation results of Usanova et al. (2016, 2018), Yu et al. (2017), H. Chen et al. (2018), and Zhu and Chen (2019), we have analyzed three types of harmonic generation associated with oscillitons. In the first case, Figures 8a and 8b, an oscilliton is considered that exists in a proton plasma with 1% admixture of O$^+$. At a selected angle $\theta = 10°$, the associated wave number is determined by kc/$\omega_p \sim 0.11$, and with an oscilliton velocity of $U = 1.01 \, V_{Ap}$, the fundamental frequency identical with the cross-over frequency is $\omega/\Omega_p = 0.11$. As can be seen from Figure 8b, two further harmonics occur at kc/$\omega_p \sim 0.22$ and kc/$\omega_p \sim 0.33$, respectively. Accordingly, the frequencies are $\omega/\Omega_p \sim 0.22$ and $\omega/\Omega_p \sim 0.33$.

A different situation arises, shown in Figures 8c and 8d, when as source of EMIC waves an oscilliton is chosen which based on the interaction of two oxygen ion populations at different temperatures. In this case the
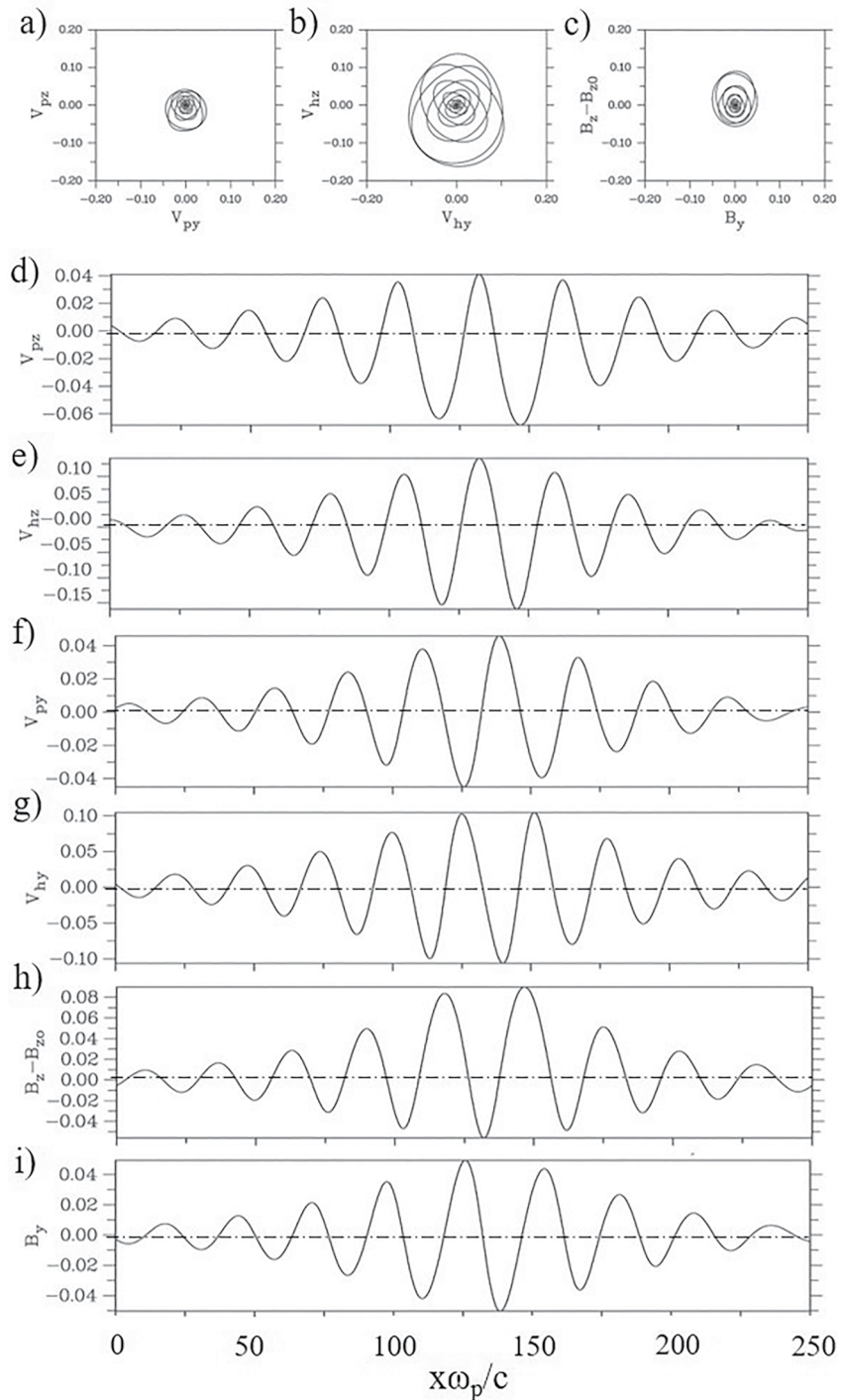
Figure 7. Oscilliton profiles as solution of the ordinary differential equations in Appendix B: Panels (a–c) represent the hodograms of the transverse proton and He$^+$ velocities and of the transverse magnetic field. In the panels below the spatial variation of the following six quantities is shown: V_{pz}, V_{hz}, V_{py}, V_{hy}, B_z-B_{z0} and B_y. Note the phase relations between each variable which has a wavelength of about $\lambda = 25c/\omega_p$.

fundamental frequency of the oscilliton is very close to the oxygen ion cyclotron frequency $\Omega_O^+ = 0.063\ \Omega_p$. Starting with the fundamental wave number of $kc/\omega_p = 0.07$, in Figure 8d more than 10 harmonics are seen. The spectral maximum at about $kc/\omega_p \sim 0.4$ is obviously caused by the existence of another oscilliton (marked by the red dashed circle) which arises due to the momentum coupling between the protons and the oxygen ion
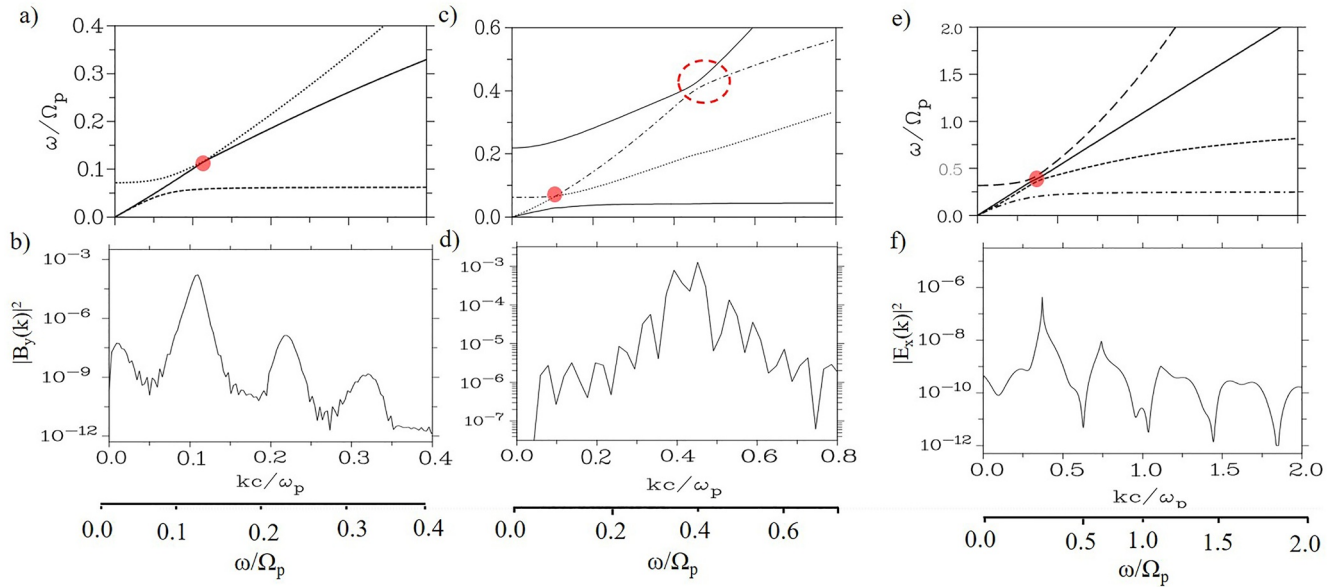
Figure 8. Harmonic generation by three kinds of oscillitons: (a and b) oscilliton caused by the momentum exchange between protons and 1% cold oxygen ions; $\theta = 10°$, $M = U/V_{Ap} = 1.01$; (c and d) oscilliton generated in a cold proton plasma with an admixture of 15% cold and 5% hot oxygen ($\beta_h = 0.1$), $U/V_{Ap} = 0.88$; (e and f) example of electrostatic cyclotron harmonics illustrating consequences of hot electrons. A plasma with 10% of (cold) He$^+$ ions is considered; $\theta = 5°$. With $\beta_e = 2.4$ an electron temperature was chosen that at the cross-over frequency the magneto-acoustic wave (solid line) squeezes itself between both the R- and L- modes. The dispersion $\omega(k)$ of the EMIC waves is shown in the panel (a, c, and e). The associated power spectrum the magnetic field component B_y is plotted in the panels (b and d). The dashed curve in panel (f) represents the electrostatic field power. The "oscilliton frequency" on the most bottom scale follows from the relation $\omega = k_r U$. The red points mark the cross-over frequencies.

populations. Considering the high number of harmonics, one has to take into account that in the fluid approach no cyclotron damping is involved.

Finally, a special case is shown in Figures 8e and 8f, which is related to the fact that the magneto-acoustic mode comes into play assuming finite electron temperatures. Otherwise, the plasma consists of protons with an admixture of 10% He$^+$. Here the special situation is shown that, in addition to the previous right- and left-hand polarized modes, the magneto-acoustic mode contributes to the formation of the oscilliton. This is achieved by an appropriate choice of the electron temperature, which is fixed by $\beta_e = 2.4$, bringing the phase velocity close to $V_{ph}/V_{Ap} = 1$. The special feature of the calculated wave number spectrum in Figure 8f is that only the fundamental wave is electromagnetic in nature and has a corresponding peak in the power spectrum of the magnetic field component (solid line). As can be seen from the dashed curve in Figure 8f, on the other side, several harmonics appear in the power spectrum of the electrostatic field component. Accordingly, these waves are linearly polarized. To what extent magneto-acoustic modes with phase velocities below the Alfven velocity, due to their coupling with the Alfven wave, can generate electrostatic harmonics in a similar way has not been further investigated by us. Further discussion follows later in connection with observations from recent satellite missions.

3. Discussion

It has been shown (Dubinin et al., 2002; Dubinin, Sauer, & Mckenzie, 2003; Dubinin, Sauer, Mckenzie, & Chanteur, 2003a, 2003b; Sauer at al. 2001, 2002; Sauer & Dubinin, 2003) that oscillitons can exist in different plasma systems in which two wave modes are superimposed at one (ω, k) point. These wave modes can be based on the existence of different particle groups, for example, electrons and ions, beams, electron and ion groups at different temperatures, etc. However, the common property is that the splitting of the associated dispersion curves by mode coupling leaves a gap region in which stationary, growing waves exist. In the end, a non-linear system results in which rotating and/or oscillating groups of particles are resonantly coupled to the electromagnetic field. The properties of these oscillitons determine the characteristics of the associated coherent waves. In this consideration, the triggering of oscillitons by instabilities initially plays a subordinate role.

So far, it has been difficult to prove this theoretical concept with well-founded measurements. However, this situation has changed with the improved technology and the possibility of multipoint measurements of very recent space missions. In addition, the analysis of low-frequency EMIC waves and the measurement of basic parameters of a multi-ion plasma is easier to realize than details of electron distribution functions when dealing with high-frequency processes, for example, in the range of whistler and Langmuir waves. In the following we will analyze the various observations about EMIC waves under the aspect, which of their properties can be explained with the concept of oscillitons as presented in Section 2.

The first characteristic quantity of our discussion is the frequency of the EMIC waves. For a magnetospheric multi-ion plasma made of protons (single charged helium and oxygen ions), three emission bands are distinguished: H^+ band between the local H^+ and He^+ cyclotron frequency, He^+ band between the local He^+ and O^+ cyclotron frequency, and O^+ band below the local O^+ cyclotron frequency, see Figure 2. There a numerous measurements that report in particular EMIC waves in the middle of the H^+ band, as by Lee et al. (2012), E.-H. Kim et al. (2015), Vines et al. (2019) and H. Chen et al. (2020). Statistical analysis of EMIC waves in the H^+ and He^+ band has carried out for example, by X.-J. Zhang et al. (2016) and Jun et al. (2019). Triggered EMIC activity in association with Pc1 waves in Cluster measurements has been described by Pickett et al. (2010). Narrow-banded EMIC waves with frequencies at $\omega \lesssim 0.5\ \Omega_p$ have also been seen by Temerin and Lysak (1984) in the S3-3 satellite electric field wave data at altitudes between 800 and 8,000 km. What is striking for EMIC activity in the H^+ band (apart from waves in the immediate vicinity of the proton cyclotron frequency Ω_p) is the absence of frequencies above ~0.5 Ω_p. This can hardly be explained by a lack of the common proton temperature-anisotropy or beam instability within this frequency range. But it seems to be in accordance with our predictions in Figure 2 according to which the "oscilliton frequency" in the H^+ band (due to a He^+ content) remains below $\omega \sim 0.45$ Ω_p as long as the corresponding abundance ratio n_{He}^+/n_H^+ remains below the reasonable value of ~0.15. As an example of statistical measurements by Jun et al. (2019), Figure 2b shows the variation in frequency of EMIC waves in the H^+ and He band over the magnetic latitude (MLAT). From the comparison with Figure 2a one can conclude that the measured maximum frequencies ($\omega/\Omega_p < 0.5$ for the H^+ band, $\omega/\Omega_p < 0.25$ for the He^+ band) are associated with a maximum content of about 20% He^+ and 7% O^+, respectively. The results of E.-H. Kim et al. (2015) and H. Chen et al. (2020) can be commented on in a similar way.

The concept of oscillitons as a source of coherent EMIC waves receives valuable support from the multi-point measurements of the four MMS satellites. Very coherent wave packets have been observed simultaneously. With the help of Wave Curl Analysis, Vines et al. (2021) determined the wave number of a coherent event in the H^+ band with the frequency $\omega/\Omega_p \sim 0.42$. From the measured component parallel to the magnetic field of $k_\parallel = 3.3 \cdot 10^{-3}$ rad/km, a normalized wave number of $k_\parallel c/\omega_p \sim 0.5$ is obtained if a proton density (not given in the paper) of $n_p = 5$ cm^{-3} is assumed. With an "oscilliton velocity" of $M = U/V_{Ap} \sim 0.8$ (according to Figure 1a) this results in an "oscilliton frequency" of the EMIC wave of $\omega \sim 0.4\ \Omega_p$ which is in good agreement with the spacecraft measurements.

Especially valuable for confirming the oscilliton concept is the evaluation of multi-point measurements by Toledo-Redondo et al. (2021). According to their interpretation, the observed EMIC waves in the H^+ band ($\omega/\Omega_p \sim 0.7$) arise from the momentum exchange of two groups of cold and warm protons via the mediating electromagnetic field. This is shown very convincingly by the measured waveforms for the corresponding proton velocities and the electric and magnetic fields which agree well with the waveforms in Figure 5d. The associated (normalized) wave number is $kc/\omega_p \sim 1$ and, with a "oscilliton velocity" of $M \sim 0.8$, supplies an "oscilliton frequency" of $\omega/\Omega_p \lesssim 1$. Adapted from Figure 2 of Toledo-Redondo et al. (2021), in Figure 9 (a) the magnetic field, (b) the velocity of the cold, and (c) the warm proton population are shown. If normalized values are used as before (ΔB in units of B_0, Δv in units of V_{Ap}), it is immediately apparent that transverse components have approximately the same amplitude of about 0.04. Furthermore, there is an opposite phase relationship between $\Delta B^\perp$ and $\Delta v_c^\perp$, that is, $\Delta B^\perp/B_0 = -\Delta v_c^\perp/V_{Ap}$, which is particularly clearly seen in the bluely marked transverse components in Figures 9a and 9b. Such a relation expresses the conservation of momentum according to Equations B7 and B8, assuming that the contribution of the warm proton population is negligible because of lower density and velocity. Further (not shown here), the transverse electric and magnetic fields follow roughly Faraday's law according to Equations B10 and B11. Finally, as a remarkable signature one has to point out that the waves are right-hand polarized both in the observations and theory. Altogether, these results support impressively the concept of oscillitons as a source of coherent EMIC waves.
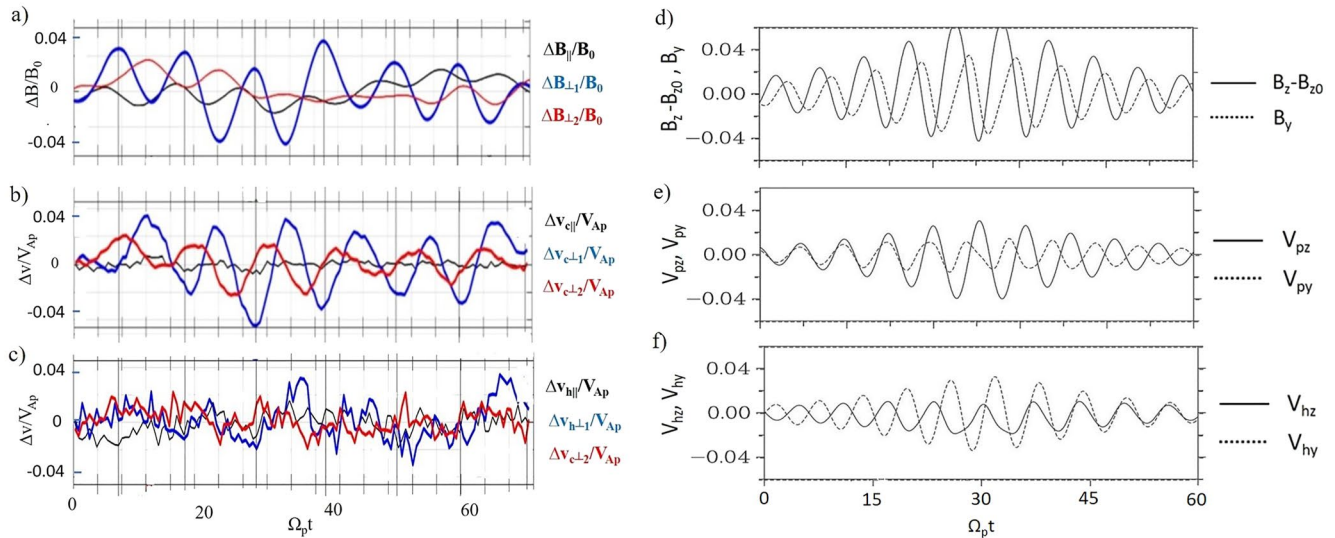
Figure 9. (a–c) Waveforms adapted from the multi-point measurements of Toledo-Redondo et al. (2021) and (d–f) spatial profiles of the proton two-temperature oscilliton of Section 2.4, see Figures 5c and 5d. The panels present: (a) the magnetic field components $\Delta B\|$ (black line), $\Delta B\perp_1$ (blue) and $\Delta B\perp_2$ (red) in units of B_0, the corresponding velocity components of (b) the cold proton and (c) of the hot population in units of V_{Ap}. The magnetic field and the proton Alfven velocity are $B_0 = 36$ nT and $V_{Ap} = 770$ km/s, respectively. In panels (d–f) the spatial profiles of the oscilliton described in Section 2.4 are shown. The corresponding two-temperature plasma consists of cold (index p) and hot protons (index h) of the same density with $\beta_h = 0.2$. The propagation angle is $\theta = 60°$.

EMIC waves in the immediate vicinity of the proton gyro frequency have also been reported by Teng et al. (2019). To what extent, according to our representations, these waves are actually based on the existence of electron groups of different temperatures, however, cannot be inferred from their measurements. The observation of stationary waveforms and the determination of the wave number of EMIC events by is also highlighted in the NASA Report 2017 (J. Zhang et al., 2017) as a key result of the mission. From the information given there ($\theta = 71.5°$, $|k| = 0.005$ km^{-1}, $\omega \sim 1.9$ s^{-1}, $V_{ph} \sim 373$ km/s) one can conclude that the observed EMIC event is based on the existence of two proton populations whose frequency is close to Ω_p.

The harmonics play a remarkable role in the interpretation of EMIC waves since their propagation properties allow important conclusions to be drawn about the properties of the plasma and the mechanism by which the fundamental wave is formed. Various observations of electromagnetic ion cyclotron harmonic (EMICH) waves are reported in the literature, These include the work of Liu et al. (1994), Usanova et al. (2016, 2018), Yu et al. (2017), H. Chen et al. (2018), Zhu and Chen (2019), and Deng et al. (2022). Consistent with our investigations, the events are differentiated by the frequency of the fundamental wave. In some cases this is almost identical to the gyro frequency, in other examples it is above or below it. When considering the relationship between EMICH waves and oscillitons, one must always keep in mind that oscillitons are based on the non-linearity of the fluid-Maxwell equations. It is therefore only natural that the properties of the oscillitons are also reflected in their harmonics.

As first example, the observation of oxygen gyro harmonics by H. Chen et al. (2018) are discussed. With a frequency of $\omega \sim 1.6$ $\Omega_O{}^+$ this event corresponds to the theoretical situation in Figures 8a and 8b where the governing oscilliton arises by the electromagnetic coupling of protons and oxygen at the cross-over point of both mixed modes in the two-ion plasma. The frequencies of the higher harmonics are n times of that of the fundamental wave. The waves propagate nearly parallel to the magnetic field, $\theta \sim 10°$, and are linearly polarized. In the work by Usanova et al. (2016) an EMICH event with frequencies very close to the harmonics of the oxygen ion cyclotron frequency is described. Noteworthy is the observation of a clear change in the direction of wave propagation at the harmonics: the waves with frequencies adjacent to multiples of the O$^+$ gyrofrequency travel on the opposite directions. This event belongs obviously to the case in Figures 4d and 5c, where the fundamental wave is an oscilliton which arises due to two coupled oxygen ion populations, consisting of a cold and a warm one. The observed splitting of the harmonics into right-hand and left-hand circular waves propagating in opposite directions suggests a slight drift between the two groups of ions. Another observation by Usanova et al. (2018) of harmonics of the oxygen ion cyclotron frequency $\Omega_O{}^+$, on the other hand, corresponds more to the previously

described event of H. Chen et al. (2018) where the fundamental EMIC wave belongs clearly to the He$^+$ band. That means, the frequency of the fundamental wave is above $\Omega_{\mathrm{O}}{}^+$ indicating, according our expectations, an oscilliton owing to proton-He+ momentum coupling as origin of the observed emission. The quasi-parallel propagation of these waves is considered as a further clue for this interpretation.

In measurements of electromagnetic oxygen ion cyclotron harmonics by Deng et al. (2022) it is has been found that the frequencies of these emissions fall around the harmonics of the specific frequency $\omega_0 \sim 2\,\Omega_{\mathrm{O}}{}^+$. This has stimulated the question whether the second harmonic plays generally a particular role in the nonlinear mechanism of harmonic generation. In this context we want to point out and refer to Figures 5a and 5b that oscillitons in a proton-He$^+$ plasma may generate harmonics whose fundamental frequency ω_0 is approximately $2\,\Omega_{\mathrm{O}}{}^+$ if the He$^+$ content is about 1%. Whether the peculiarity that the oscilliton frequency is actually in the range of the second harmonic of $\Omega_{\mathrm{O}}{}^+$, can only be clarified by appropriate plasma measurements.

With the observation of electrostatic harmonics by Zhu and Chen (2019) a particular type of harmonic generation in association with EMIC waves is reported which is essentially different from the electromagnetic events above. Whereas the fundamental wave is located in the He$^+$ band and of electromagnetic nature is, the third harmonic and above (up to fifth) are above the proton cyclotron frequency and have only electric field components (without magnetic fluctuations) propagating bi-directional with respect to the magnetic field. In order to fulfill the resonance conditions (the ω, k relations) a plasma wave mode is required which is essentially electrostatic. In the low-frequency range of EMIC waves that can only be the magneto-acoustic mode with a dispersion of $\omega = C\,k$, where C is the (constant) phase velocity. Such a case has been considered in our power spectrum analysis of Figures 8e and 8f. For the selected electron temperature of $\beta_e = 2.4$ the magneto-acoustic mode with $C = V_{\mathrm{ph}} \sim (\beta_e/2)\,V_{\mathrm{Ap}}$ touches the crossing (oscilliton) point of the proton-He$^+$ plasma at $\omega \sim 0.4\,\Omega_p$ ($kc/\omega_p \sim 0.4$), see Figure 8e. This condition enables obviously the generation of four and more electrostatic harmonics. We are not sure whether in the event of Zhu and Chen (2019) a plasma with hot electrons of $\beta_e = 2.4$ really exist. From a theoretical point of view, it is challenging to find out whether other particle populations such as groups of hot or accelerated electrons or ions can give rise to a magneto-acoustic mode whose phase velocity is also close to the proton Alfven velocity to be favorable to touch the ω-k region of spatially growing waves.

A more complex problem concerns the interpretation of the polarization of the observed EMIC waves in relation to our model of oscillitons. It is difficult to derive a consistent picture from the literature. For example, adjacent lines can be polarized differently, as for example, in the measurements by H. Chen et al. (2018). However, it remains to be seen that linear polarization is present in the majority of the analyzed events, with left polarization appearing to be somewhat more strongly represented, see E.-H. Kim et al. (2015), Vines et al. (2019), and Jun et al. (2021). Regarding the polarization of EMIC waves, from the theoretical point of view one has to take into account two aspects. On the one hand, in the source region i.e., the region where EMIC waves are driven by the temperature instability, left-hand polarized waves should dominate. Furthermore, based on the simulation results for Langmuir-whistler oscillitons in Appendix C, one can conclude that simultaneously with the instability EMIC oscillitons are triggered, the polarization of which ultimately depends on the proportion of heavy ions in the plasma. Therefore, in the source region, one has to reckon with the fact that a complex picture of the polarization arises as a result of the superimposition of both wave types. Outside the source region, however, one can assume that the polarization is determined by the oscillitons, whose polarization would change from LH (near the equator) to RH polarization (in the region of higher latitudes) as the admixture of heavy ions decreases. Such a variation was observed in the statistical measurements for example, by Jun et al. (2021). A compelling example of RH polarized EMIC waves one finds for example, in the work of Nakamura et al. (2014). The observed wave activity in the H$^+$ band with $\omega \sim 0.3\,\Omega_p$ and at a propagation angle of $\theta \lesssim 30°$ is obviously related the presence of a small abundance of He$^+$ ($\sim$2%) which well agrees with our considerations in Section 2.4. Not surprisingly, the EMIC waves occurring simultaneously in the He$^+$ band ($\omega \sim 0.1\,\Omega_p$) show RH polarization, what can be associated with an O$^+$ abundance of 1–2 percent.

There remains the discussion of the amplitudes of oscillitons. In the case of the two-temperature proton plasma shown in Figure 9 we found a good agreement between the measurements by Toledo-Redondo et al. (2021) and the outcome of the oscilliton theory. The situation is not so satisfactory if heavy ions are involved. Crucial quantity in the simplest model of cold multi-ion oscillitons is the density of the individual ion components in relation to the proton density. In parameter studies we found that the calculated amplitudes are generally about one order of magnitude higher than the measured values. As seen in Figures 5a and 5b, for a plasma with 10% of

helium and 5% of oxygen the velocity and magnetic field disturbances are of the order $\Delta v/V_{Ap} \sim \Delta B/B_0 \sim 0.1$. In the measurements, for example, by Vines et al. (2021), one the other hand, one only finds $\Delta B/B_0 \lesssim 0.01$. Whether this discrepancy indicates a smaller heavy ion abundance or other effects remains open. In all these considerations, however, one must always keep in mind that the fluid description of EMIC oscillitons can only represent a very rough model of the real conditions. A first extension could be a kinetic dispersion theory of stationary waves, which could be worked out with reasonable effort. Such an approach would significantly reduce the spatial growth rates due to kinetic damping effects. Ultimately, you have to use simulations, for example, in the form of hybrid codes, to check the simple models.

A final but very important point of discussion concerns the role of instabilities in the formation of multi-ion oscillitons as the source of coherent waves in the plasma. Results of an instability analysis in a proton-He$^+$ with temperature-anisotropy are presented for example, in the paper by L. Chen et al. (2011). Instabilities are involved in the process of oscilliton formation in two ways. In the first case, they are responsible for triggering the oscillitons when the conditions for their existence are present. This means that the instabilities are the reason why the system of two particle populations and the connecting electromagnetic field starts to oscillate. In the (ω, k) space this happens at the cross-over points, where phase and group velocities are the same. It is worth noting that these points are generally different from those of maximum instability. Another situation occurs when the instability, for example, due to wave-particle heating, creates a second particle group that differs from the already existing one due to different temperature or speed, for example, Teng et al. (2019), Usanova (2021), and Toledo-Redondo et al. (2021). In this case, oscillitons can arise in which groups of particles with the same mass participate, but which differ from each other in other parameters. Finally, oscillitons and waves with the frequencies in the neighborhood of the maximum growth rate can exist simultaneously, as shown, for example, for Langmuir-whistler oscillitons discussed in the Appendix.

4. Summary

Multi-ion oscillitons are stationary nonlinear waves which arise at the mode crossing points of the obliquely propagating electromagnetic waves in plasmas with several ion populations. In these (Gendrin) points the phase and group velocity of the coupled waves coincide and it is used as reference velocity of the moving frame in deriving the set of stationary nonlinear Hall-MHD equations.

The main results of our studies are the following:

1. The frequency of the EMIC oscillitons is close to the corresponding heavy-ion cyclotron frequency and increases with growing abundance ratio. For He$^+$ admixture of slightly above 10% a oscilliton frequency of about 0.4 Ω_p is gained. A 5% portion of oxygen ions results in a frequency of about 0.2 Ω_p.
2. With decreasing heavy-ion density the optimum conditions of oscilliton generation shift to larger propagation angles which is associated with a change of polarization from RH to LH polarization. For an abundance of 1% He$^+$, for example, RH polarized oscillitons have been found at $\theta = 30°$ with a frequency of about 0.25 Ω_p.
3. RH polarized oscillitons of frequencies close to Ω_p have been seen in a plasma with cold and hot proton populations of the same density.
4. Harmonics of the EMIC oscilliton frequency have been obtained for different plasma compositions. For example, more than five harmonics of the oxygen cyclotron frequency Ω_{O^+} appeared in a He$^+$ - O$^+$ plasma.
5. As a very specific case, it has been shown that He$^+$ oscilliton harmonics of electrostatic nature may exist, similar as described by Zhu and Chen (2019). For their formation it is necessary that the magneto-acoustic mode is involved in the momentum exchange with the magnetic field of the resulting electromagnetic wave. Further experimental and theoretical studies are required to find out which particle populations are involved in the existence of the electrostatic wave mode.
6. It is suggested that the EMIC oscillitons can be triggered by the cyclotron instability of protons owing to a temperature anisotropy. That means, two kinds of EMIC waves can be present in the source region: unstable left-hand polarized waves and EMIC oscillitons with variable polarization. Outside the source region only oscillitons can survive.

Kinetic studies on the basis of Vlasov theory and particle simulations are required to complete the oscilliton concept of coherent magnetospheric EMIC waves.

5. Conclusions

In conclusion, we would like to express that the described investigations of multi-ion oscilltons in the magnetosphere can be fully transferred to comparable situations in other plasma environments. This applies in particular to the plasmas in the vicinity of comets and non-magnetized planets, where the interaction of the solar wind with the locally generated ions leads to complex wave phenomena in the low-frequency range (Halekas et al., 2020; Mazelle et al., 2004; Nagy et al., 2004; Tsurutani, 1991). But also the solar wind itself is a laboratory for the investigation of multi-ion structures due to its composition of different proton groups (core and halo) and the admixture of alpha particles. In this context, the recent measurements of the Solar Orbiter of coherent proton cyclotron frequency waves of both polarizations (RH and LH) are worth mentioning (Khotyaintsev et al., 2021). Referring to Figures 5c and 5d, the conclusion is obvious that two different proton populations are involved in the formation of the observed nonlinear structures.

Finally, regarding the momentum exchange between electrons, similar conditions can also prevail in the frequency range of the whistler waves and lead to whistler oscillitons in a plasma with electron populations of different temperatures (not described so far), which are different from the whistler oscillitons at $\omega \sim \Omega_e/2$ due to the electron-proton coupling (Dubinin, Sauer, & Mckenzie, 2003; Sauer et al., 2002). Such a kind of two-temperature oscilltons may explain the observed whistler wave packets ($\omega < \Omega_e/2$) in the magnetosphere (Dubinin et al., 2007) and in the solar wind (Breneman et al., 2010) and of chorus waves in the magnetosphere (Tsurutani et al., 2009, 2020).

Appendix A: Hall-MHD Equations

The governing system of Hall-MHD equations on which the theory of oscilltons is based is the following, using standard notations:

The continuity equation and equation of motion of ions, p, h and i stands for protons, He$^+$ ions and O$^+$ ions, respectively.

$$\frac{\partial}{\partial t} n_j + \nabla \cdot (n_j \mathbf{v}_j) = 0 \tag{A1}$$

$$\frac{\partial}{\partial t} (n_j \mathbf{v}_j) + \nabla \cdot \left(n_j \mathbf{v}_j \mathbf{v}_j + \frac{p_j}{n_j m_j} \right) = \frac{q_j n_j}{m_j} \left(\mathbf{E} + \mathbf{v}_j \times \mathbf{B} \right), \quad j = \mathrm{p, h, i} \tag{A2}$$

p_j is the thermal pressure, $p_j = \gamma\, n_j\, \kappa\, T_j$.

With the assumption of massless electrons the equation of motion for the electrons is reduced to

$$\frac{1}{n_e} \nabla \cdot p_e = -e \left(\boldsymbol{E} + \mathbf{v}_e \times \mathbf{B} \right) \tag{A3}$$

The electron density n_e follows via charge neutrality:

$$n_e = n_p + n_h + n_i. \tag{A4}$$

Together with Faraday's law

$$\frac{\partial}{\partial t} \mathbf{B} + \nabla \times \mathbf{E} = 0 \tag{A5}$$

and Ampere's law

$$\nabla \times \mathbf{B} = \mu_0 \boldsymbol{j} \tag{A6}$$

where the current is given by

$$\boldsymbol{j} = e(n_p \mathbf{v}_p +) n_h \mathbf{v}_h + n_i \mathbf{v}_i - n_e \mathbf{v}_e) \tag{A7}$$

one gets a closed system of equations.

Appendix B: Oscilliton Equations for a Cold Two-Ion Plasma

In order to analyze the nonlinear, stationary spatially oscillating structures (oscillitons) which may arise in the frequency gaps near the cross-over points of multi-ion plasmas, a one-dimensional model is considered. The *x*-axis is in the propagation direction of the wave; the magnetic field is located in the x-z plane with an angle θ with respect to the *x*-axis, that is, $\mathbf{B}_0 = (B_0\cos\theta, 0, B_0\sin\theta)$. Looking for stationary waves, all variables $f(x,t)$ with respect to the time dependence are considered as function of $x' = x - Ut: f = f(x, x - Ut)$ where U is the velocity of the moving structure. Thus, the convective derivative $D/Dt = \partial/\partial t + u_{ix}\,\partial/\partial x \rightarrow (-U + u_{ix})\partial/\partial x$.

The resulting system equations which describes the simplest kind of oscillitons in a cold two-ion plasma is given below. The plasma under consideration consists of cold electrons and two cold ion populations, protons (index p) and single-charged helium (index i). All quantities are written in units of the protons, that means $n_i = n_{He}{}^+/n_{po}$ is the normalized He^+ density, where n_{po} is the undisturbed proton density. The mass is in units of the proton mass m_p, that is, $m_i = m_{He}{}^+/m_p = 4$. The velocities are normalized with the proton Alfven velocity $V_{Ap} = B_0/(\mu_0 n_{po} m_p)^{1/2}$, the magnetic field is in units of B_0. Thus, the normalized "oscilliton velocity" is given by $M = U/V_{Ap}$ and the unit of the electric field is $E_0 = V_{Ap}B_0$.

To determine the 17 variables (n_p, n_i, n_e, $\mathbf{v}_p$, $\mathbf{v}_i$, $\mathbf{v}_e$, B_y, B_z, E_x, E_y, E_z) our system of equations consists of six differential equations and 11 algebraic relations. The latter result either directly from the assumption of massless electrons and charge neutrality or they are the result of the integration of the (stationary) Hall-MHD equations. The system of equations can be written as follows:

$$\frac{dv_{iy}}{dx} = \frac{1}{m_i}\left[\frac{n_{i0}B_z - n_iB_{z0}}{n_{i0}} + \frac{n_iv_{iz}B_x}{n_{i0}M}\right] \tag{B1}$$

$$\frac{dv_{iz}}{dx} = \frac{1}{m_i}\left[B_y + \frac{n_iv_{iy}B_x}{n_{i0}M}\right] \tag{B2}$$

$$\frac{dB_y}{dx} = -n_ev_{ez} + n_pv_{pz} + n_iv_{iz} \tag{B3}$$

$$\frac{dB_z}{dx} = -\left(-n_ev_{ey} + n_pv_{py}\right) \tag{B4}$$

$$\frac{dn_p}{dx} = \frac{n_p^3}{M^2}\frac{n_i}{n_e}\left[\left(v_{py} - v_{iy}\right)B_z - \left(v_{pz} - v_{iz}\right)B_y\right] - \frac{B_y{}^{dB_y}/_{dx} + B_z{}^{dB_z}/_{dx}}{n_e} \tag{B5}$$

$$\frac{dn_i}{dx} = -\frac{n_i^3}{n_{io}^2 M^2 m_i}\frac{n_p}{n_e}\left[\left(v_{py} - v_{iy}\right)B_z - \left(v_{pz} - v_{iz}\right)B_y\right] - \frac{B_y{}^{dB_y}/_{dx} + B_z{}^{dB_z}/_{dx}}{m_i n_e} \tag{B6}$$

$$v_{pz} = -n_{io}\, m_i v_{iz} - \frac{B_x(B_z - B_{z0})}{M} \tag{B7}$$

$$v_{py} = -n_{io}m_i v_{iy} - \frac{B_xB_y}{M} \tag{B8}$$

$$E_x = -\left(v_{ey}B_z - v_{ez}B_y\right) \tag{B9}$$

$$E_y = M(B_z - B_{z0}) \tag{B10}$$

$$E_z = -MB_y \tag{B11}$$

$$v_{ex} = \left(n_pv_{px} + n_iv_{ix}\right)/n_e \tag{B12}$$

$$v_{ey} = -\frac{M}{B_xn_e}n_{e0}B_y \tag{B13}$$

$$v_{ez} = -\frac{M}{B_xn_e}\left(n_{e0}B_z - n_eB_{z0}\right) \tag{B14}$$

$$v_{px} = M\left(n_p - 1\right)/n_p \tag{B15}$$

$$v_{ix} = M(n_i - n_{i0})/n_i \tag{B16}$$

$$n_e = n_p + n_i \tag{B17}$$

Appendix C: Langmuir-Whistler Oscillitons and Proposed Simulation of EMIC Oscillitons

After the discussion of EMIC wave events in space (Section 3) which are related to the concept of multi-ion oscillitions, we want to address the possibilities of particle simulations by which the generation of oscillitons and their triggering by instabilities can be investigated.

Owing to the lack of particle simulations to EMIC oscillitons, as a first step, it seems to be useful to draw conclusions from another type of oscillitons, namely the so-called Langmuir-whistler oscillitons (Sauer & Sydora, 2011, 2012), for which particle-in-cell (PIC) simulations have been done. Although these oscillitons exist in the frequency range much higher than the EMIC waves, fundamental connections between instability
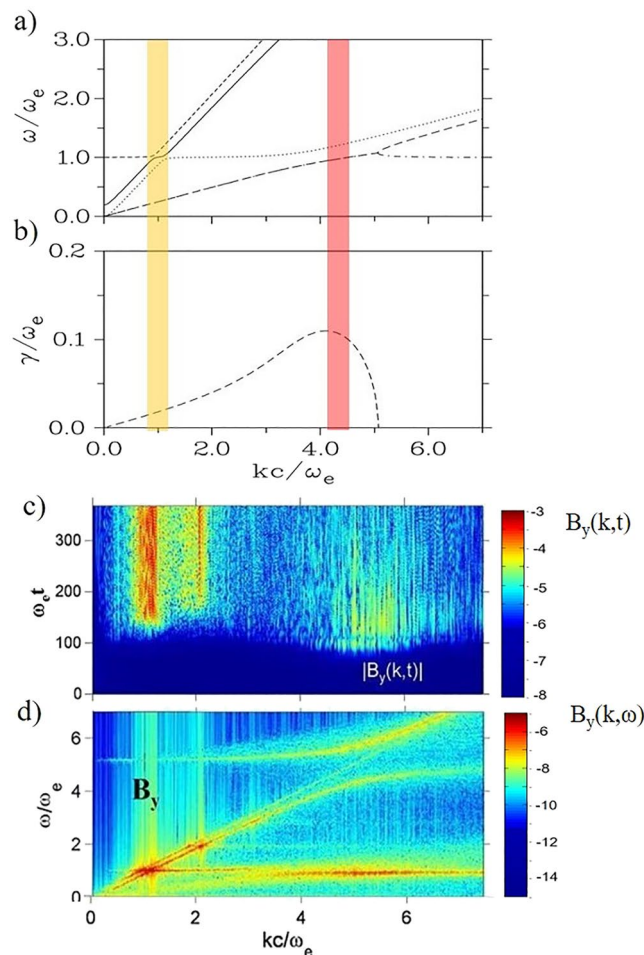

Figure C1. Dispersion of electromagnetic waves (a–c) in a cold under-dense plasma ($\Omega_e/\omega_e = 5$) at oblique propagation driven by an electron beam with a beam velocity of $V_b/c = 0.25$ and results of PIC simulations (c and d) as indication of Langmuir-whistler oscilliton. In (a) - frequency versus k – the electromagnetic R-mode (lower branch: whistler wave), the electromagnetic L-mode, the Langmuir mode at $\omega \sim \omega_e$ and the beam mode $\omega \sim kV_b$ are seen. Panel (b) shows the growth rate γ/ω_e versus kc/ω_e. Panel (c) represents the temporal evolution of the magnetic field component $B_y(k)$; (d) shows the (ω, k) spectrum of B_y. Note the pronounced wave activity at the mode crossing point ($\omega/\omega_e \sim 1$, $kc/\omega_e \sim 1$) which indicates the generation of the Langmuir-whistler oscilliton, s.a. Sauer and Sydora (2011).

and stationary waves can be derived from them. Essential information for understanding the Langmuir-whistler oscillitons is given in Figure C1. Electromagnetic waves in a (cold) under-dense plasma ($\Omega_e = 5\,\omega_e$) at oblique propagation ($\theta = 5°$) are considered. Their dispersion ω versus k shown in panel (a) is described in more detail in Baumjohann and Treumann (1996), for example, In addition, an electron beam with a beam density of $n_b/n_0 = 0.01$ and a speed of $V_b = 0.25c$ is assumed by which electron plasma waves ($\omega \sim \omega_e$) are excited. According to panel (b), showing the growth rate γ/ω_e versus kc/ω_e, maximum instability appears at $kc/\omega_e \sim 4$. The region of the beam instability is marked in panels (a and b) by the red bar. The yellow bar in both panels, on the other hand, marks the wave number range in which the electromagnetic modes cross the Langmuir mode, which in oblique propagation is associated with mode splitting and creation of a Gendrin point (Gendrin, 1961) where phase and group velocity coincide (Sauer & Sydora, 2011). How the two signatures of the dispersion theory (maximum instability and Gendrin point) are reflected in the PIC simulations can be seen in Figures C1c and C1d. Figure C1c shows the temporal evolution of the magnetic field component $B_y(k)$ up to $\omega_e t = 350$. Considering the beam instability around its maximum at $kc/\omega_e \sim 5$, saturation is reached at about $\omega_e t = 100$. Afterward the amplitude of $B_y(k)$ decreases continually. A remarkable feature, in addition, is the occurrence of another maximum in $B_y(k)$ just at the Gendrin point at $kc/\omega_e \sim 1$ even larger than the value resulting from the beam instability at $kc/\omega_e \gtrsim 4$. These waves represent the Langmuir-whistler oscillitons (Sauer & Sydora, 2011). The slightly fainter line at $kc/\omega_e \sim 2$ represents the second harmonic associated with the Langmuir-whistler
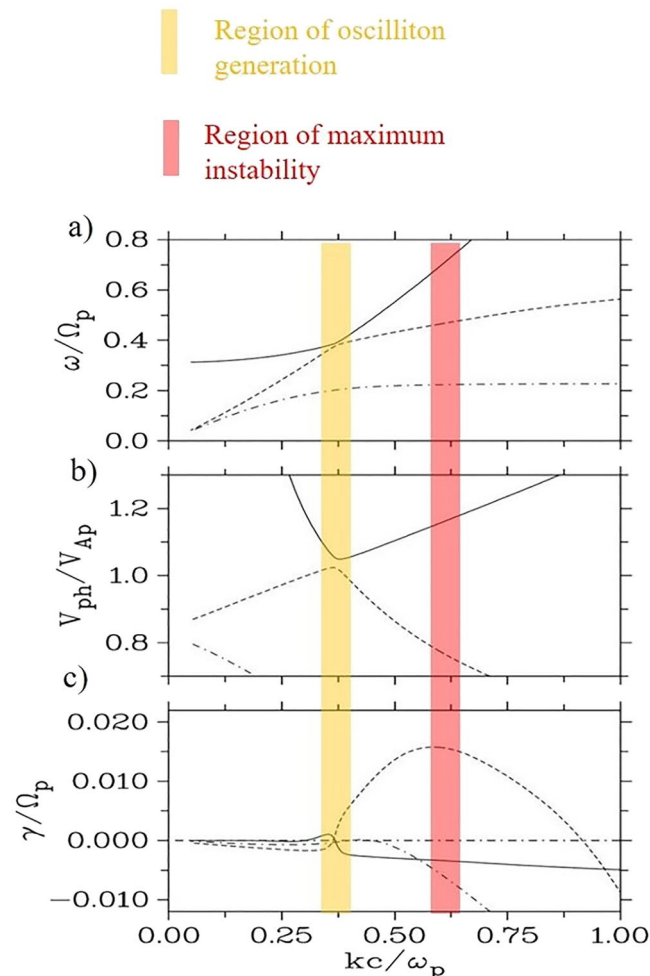

Figure C2. Dispersion characteristics of a two-ion plasma with temperature anisotropy which is proposed for hybrid code simulations of EMIC oscillitons. The plasma consists of cold ($n_c/n_0 = 0.85$, $\beta_c = 0.05$), hot anisotropy protons ($n_h/n_0 = 0.1$, $T_h/T_c = 15$, $A_h = 1.8$) and cold He$^+$-ions ($n_{He}^+ = 0.1$, $T_{He}^+/T_c = 0.1$). The propagation angle is $\theta = 15°$. Maximum instability appears at $kc/\omega_p \sim 0.67$ ($\omega/\omega_p \sim 0.5$). From the point of maximum phase velocity, the generation of an EMIC oscilliton at ($kc/\omega_p \sim 0.67$, $\omega/\omega_e \lesssim 0.4$) is expected.

oscilliton by wave-wave interaction. The three wave activities (beam instability, Langmuir-whistler oscilliton and its second harmonic) also stand out clearly in the ω-k spectrum of B_y in Figure C1d by the red colored areas.

Based on the discussions above, a hybrid code simulation for the investigation of oscillitons in multi-ion plasmas is proposed as an example. As seen in Figure 8, with respect to the dispersion characteristics a similar situation as for the high-frequency whistler and Langmuir waves in Figures C1a and C1b exists for EMIC waves in a proton-He$^+$ plasma where the waves are excited by temperature anisotropy as discussed for example, by L. Chen et al. (2011). The detailed parameters are given in the caption of Figure C2. The two essential signatures are the separate regions of maximum instability (red bar) and mode splitting (yellow bar). Correspondingly, two major wave activities are expected during the temporal evolution of the instability similar as for Langmuir-whistler oscillitons: (a) One due to the instability of the Alfven mode at kc/ω_p ∼ 0.67 (red bar) and (b) the other as EMIC oscilliton at kc/ω_e ∼ 0.37 where the phase velocity (panel b) has a maximum (Gendrin point). Probably, the second harmonic of the EMIC oscilliton at ω ∼ 0.8 Ω_p will be generated too. Such a proposed hybrid code simulation would be an very important tool to study the basic mechanisms of the EMIC wave generation by a temperature anisotropy, especially the relation between instability and oscilliton.

Data Availability Statement

The paper is theoretical and does not use external data.

References

Baumjohann, W., & Treumann, R. A. (1996). *Basic space plasma physics*. Imperial College Press.

Baumjohann, W., Treumann, R. A., Georgescu, F., Haerendel, G., Fornacon, K.-H., & Auster, U. (1999). Waveform and packet structure of lion roars. *Annales Geophysicae*, *17*(12), 1528–1534. https://doi.org/10.1007/s00585-999-1528-9

Breneman, A., Cattell, C., Schreiner, S., Kersten, K., Wilson, L. B., III, Kellogg, P., et al. (2010). Observations of large-amplitude, narrowband whistlers at stream interaction regions. *Journal of Geophysical Research*, *115*(A8), A08104. https://doi.org/10.1029/2009JA014920

Chen, H., Gao, X., Lu, Q., Tsurutani, B. T., & Wang, S. (2020). Statistical evidence for EMIC wave excitation driven by substorm injection and enhanced solar wind pressure in the Earth's magnetosphere: Two different EMIC wave sources. *Geophysical Research Letters*, *47*(21), e2020GL090275. https://doi.org/10.1029/2020GL090275

Chen, H., Gao, X., Lu, Q., & Wang, S. (2018). In situ observations of harmonic Alfvén waves and associated heavy ion heating. *The Astrophysical Journal*, *859*(2), 120. https://doi.org/10.3847/1538-4357/aabee2

Chen, L., Thorne, R. M., & Bortnik, J. (2011). The controlling effect of ion temperature on EMIC wave excitation and scattering. *Geophysical Research Letters*, *38*(16), L16109. https://doi.org/10.1029/2011GL048653

Deng, D., Yuan, Z., Huang, S., Xue, Z., Huang, Z., & Yu, X. (2022). Electromagnetic ion cyclotron harmonic waves generated via nonlinear wave-wave couplings. *Geophysical Research Letters*, *49*(4), e2021GL097143. https://doi.org/10.1029/2021GL097143

Dubinin, E., Sauer, K., & McKenzie, J. F. (2002). Solitons and oscillitons in cold bi-ion plasmas: A parameter study. *Journal of Plasma Physics*, *68*(1), 27–52. https://doi.org/10.1017/s0022377802001745

Dubinin, E., Sauer, K., & Mckenzie, J. F. (2003). Nonlinear stationary waves and whistler oscillitons. Exact solutions. *Journal of Plasma Physics*, *69*(4), 305–330. https://doi.org/10.1017/s0022377803002319

Dubinin, E., Sauer, K., & Mckenzie, J. F. (2004). Nonlinear stationary waves and solitons in ion beam-plasma configuration. *Journal of Geophysical Research*, *109*(A2), A02208. https://doi.org/10.1029/2003JA010283

Dubinin, E., Sauer, K., Mckenzie, J. F., & Chanteur, G. (2003a). Solitons, oscillitons, and stationary waves in a warm *p*-α plasma. *Journal of Geophysical Research*, *108*(A7), 1293. https://doi.org/10.1029/2002JA009572

Dubinin, E., Sauer, K., Mckenzie, J. F., & Chanteur, G. (2003b). Stationary waves and solitons in a cold *p*-α plasma. *Journal of Geophysical Research*, *108*(A7), 1295. https://doi.org/10.1029/2002JA009571

Dubinin, E. M., Maksimovic, M., Cornilleau-Wehrlin, N., Fontaine, D., Travnicek, P., Mangeney, A., et al. (2007). Coherent whistler emissions in the magnetosphere – Cluster observations. *Annales Geophysicae*, *25*(1), 303–315. https://doi.org/10.5194/angeo-25-303-2007

Fazakerley, A. N., Coates, A. J., & Dunlop, M. W. (1995). Observations of upstream ions, solar wind ions and electromagnetic waves in the Earth's foreshock. *Advances in Space Research*, *15*(8–9), 103–106. https://doi.org/10.1016/0273-1177(94)00091-e

Fuselier, S. A., Thomsen, M. F., Gosling, J. T., Bame, S. J., & Russell, C. T. (1986). Gyrating and intermediate ion distributions upstream from the Earth's bow shock. *Journal of Geophysical Research*, *91*(A1), 91–99. https://doi.org/10.1029/ja091ia01p00091

Gary, S. P., Scime, E. E., Phillips, J. L., & Feldman, W. C. (1994). The whistler heat flux instability: Threshold conditions in the solar wind. *Journal of Geophysical Research*, *99*(A12), 23391–23399. https://doi.org/10.1029/94JA02067

Gendrin, R. (1961). Le guidage des whistlers par le champ magnetique. *Planetary and Space Science*, *5*(4), 274–282. https://doi.org/10.1016/0032-0633(61)90096-4

Halekas, J. S., Ruhunusiri, S., Vaisberg, O. L., Harada, Y., Espley, J. R., Mitchell, D. L., et al. (2020). Properties of plasma waves observed upstream from Mars. *Journal of Geophysical Research: Space Physics*, *125*(9), e2020JA028221. https://doi.org/10.1029/2020JA028221

Huba, J. D. (2003). Hall magnetohydrodynamics - A tutorial. In J. Büchner, M. Scholer, & C. T. Dum (Eds.), *Space Plasma Simulation*. *Lecture Notes in Physics* (Vol. 615). Springer. https://doi.org/10.1007/3-540-36530-3_9

Jun, C.-W., Miyoshi, Y., Kurita, S., Yue, C., Bortnik, J., Lyons, L., et al. (2021). The characteristics of EMIC waves in the magnetosphere based on the Van Allen Probes and Arase observations. *Journal of Geophysical Research: Space Physics*, *126*(6), e2020JA029001. https://doi.org/10.1029/2020JA029001

Jun, C.-W., Yue, C., Bortnik, J., Lyons, L. R., Nishimura, Y. T., & Kletzing, C. A. (2019). EMIC wave properties associated with and without injections in the inner magnetosphere. *Journal of Geophysical Research: Space Physics*, *124*(3), 2029–2045. https://doi.org/10.1029/2018JA026279

Khotyaintsev, Y. V., Graham, D. B., Vaivads, A., Steinvall, K., Edberg, N. J. T., Eriksson, A. I., et al. (2021). Density fluctuations associated with turbulence and waves: First observations by Solar Orbiter. *Astronomy & Astrophysics*, *656*, A19. https://doi.org/10.1051/0004-6361/202140936

Kim, E.-H., Johnson, J. R., Kim, H., & Lee, D.-H. (2015). Inferring magnetospheric heavy ion density using EMIC waves. *Journal of Geophysical Research: Space Physics*, *120*(8), 6464–6473. https://doi.org/10.1002/2015JA021092

Kim, T. K., Ebert, R. W., Valek, P. W., Allegrini, F., McComas, D. J., Bagenal, F., et al. (2020). Survey of ion properties in Jupiter's plasma sheet: Juno JADE-I observations. *Journal of Geophysical Research: Space Physics*, *125*(4), e2019JA027696. https://doi.org/10.1029/2019JA027696

Lee, J. H., Chen, L., Angelopoulos, V., & Thorne, R. M. (2012). THEMIS observations and modeling of multiple ion species and EMIC waves: Implications for a vanishing He$^+$ stop band. *Journal of Geophysical Research*, *117*(A6), A06204. https://doi.org/10.1029/2012JA017539

Li, X., & Habbal, S. R. (2001). Damping of fast and ion cyclotron oblique waves in the multi-ion fast solar wind. *Journal of Geophysical Research*, *106*, 10669–10680. https://doi.org/10.1029/2000JA000420

Liu, H., Kokubun, S., & Hayashi, K. (1994). Equatorial electromagnetic emission with discrete spectra near harmonics of oxygen gyrofrequency during magnetic storm. *Geophysical Research Letters*, *21*(3), 225–228. https://doi.org/10.1029/93GL02836

Mazelle, C., Winterhalter, D., Sauer, K., Trotignon, J. G., Acuna, M., Baumgartel, K., et al. (2004). Bow shock and upstream phenomena at Mars. *Space Science Reviews*, *111*(1/2), 115–181. https://doi.org/10.1023/b:spac.0000032717.98679.d0

McKenzie, J. F., Dubinin, E., Sauer, K., & Doyle, T. (2004). The application of the constants of motion to nonlinear stationary waves in complex plasmas: A unified fluid dynamic viewpoint. *Journal of Plasma Physics*, *70*(4), 431–462. https://doi.org/10.1017/s0022377803002654

Nagy, A. F., Winterhalter, D., Sauer, K., Cravens, T. E., Brecht, S., Mazelle, C., et al. (2004). The plasma environment of Mars. *Space Science Reviews*, *111*(1/2), 33–114. https://doi.org/10.1023/b:spac.0000032718.47512.92

Nakamura, S., Omura, Y., Machida, S., Shoji, M., Nosé, M., & Angelopoulos, V. (2014). Electromagnetic ion cyclotron rising tone emissions observed by THEMIS probes outside the plasmapause. *Journal of Geophysical Research: Space Physics*, *119*(3), 1874–1886. https://doi.org/10.1002/2013JA019146

Pickett, J. S., Grison, B., Omura, Y., Engebretson, M. J., Dandouras, I., Masson, A., et al. (2010). Cluster observations of EMIC triggered emissions in association with Pc1 waves near Earth's plasmapause. *Geophysical Research Letters*, *37*(9), L09104. https://doi.org/10.1029/2010GL042648

Rauch, J. L., & Roux, A. (1982). Ray tracing of ULF waves in a multicomponent magnetospheric plasma: Consequences for the generation mechanism of ion cyclotron waves. *Journal of Geophysical Research*, *87*(A10), 8191–8198. https://doi.org/10.1029/JA087iA10p08191

Rubin, M., Combi, R., Daldorff, K., Gombosi, T., Hansen, K. C., Shou, Y., et al. (2014). Comet 1P/Halley multifluid MHD model for the Giotto fly-by. *The Astrophysical Journal*, *781*(2), 86. https://doi.org/10.1088/0004-637X/781/2/86

Sauer, K., Bogdanov, A., & Baumgärtel, K. (1994). Evidence of an ion composition boundary (protonopause) in bi-ion fluid simulations of solar wind mass loading. *Geophysical Research Letters*, *21*(20), 2255–2258. https://doi.org/10.1029/94gl01691

Sauer, K., & Dubinin, E. (2003). Oscillitons and gyrating ions in a beam-plasma system. *Geophysical Research Letters*, *30*(23), 2192. https://doi.org/10.1029/2003GL018266

Sauer, K., Dubinin, E., & McKenzie, J. F. (2001). New type of soliton in bi-ion plasmas and possible implications. *Geophysical Research Letters*, *28*(18), 3589–3592. https://doi.org/10.1029/2001GL013047

Sauer, K., Dubinin, E., & McKenzie, J. F. (2002). Wave emission by whistler oscillitons: Application to "coherent lion roars". *Geophysical Research Letters*, *29*(24), 2226. https://doi.org/10.1029/2002GL015771

Sauer, K., Dubinin, E., & McKenzie1, J. F. (2003). Solitons and oscillitons in multi-ion space plasmas. *Nonlinear Processes in Geophysics*, *10*(1/2), 121–130. https://doi.org/10.5194/npg-10-121-2003

Sauer, K., & Sydora, R. D. (2010). Beam-excited whistler waves at oblique propagation with relation to STEREO radiation belt observations. *Annales Geophysicae*, *28*(6), 1317–1325. https://doi.org/10.5194/angeo-28-1-2010

Sauer, K., & Sydora, R. D. (2011). Whistler-Langmuir oscillitons and their relation to auroral hiss. *Annales Geophysicae*, *29*(10), 1739–1753. https://doi.org/10.5194/angeo-29-1739-2011

Sauer, K., & Sydora, R. D. (2012). Mode crossing effects at electron beam plasma interaction and related phenomena. *Plasma Physics and Controlled Fusion*, *54*(12), 124045. https://doi.org/10.1088/0741-3335/54/12/124045

Smith, R. L., & Brice, N. (1964). Propagation in multicomponent plasma. *Journal of Geophysical Research*, *69*(23), 5029–5040. https://doi.org/10.1029/jz069i023p05029

Stix, T. H. (1992). *Waves in plasmas*. American Institute of Physics.

Temerin, M., & Lysak, R. L. (1984). Electromagnetic ion cyclotron mode (ELF) waves generated by auroral electron precipitation. *Journal of Geophysical Research*, *89*(A5), 2849–2859. https://doi.org/10.1029/ja089ia05p02849

Teng, S., Li, W., Tao, X., Ma, Q., Wu, Y., Capannolo, L., et al. (2019). Generation and characteristics of unusual high frequency EMIC waves. *Geophysical Research Letters*, *46*(24), 14230–14238. https://doi.org/10.1029/2019GL085220

Thompson, P., Dougherty, M. K., & Southwood, D. J. (1995). Wave behaviour near critical frequencies in cold bi-ion plasmas. *Planetary and Space Science*, *43*(5), 625–634. https://doi.org/10.1016/0032-0633(94)00197-y

Thomsen, M. F., Reisenfeld, D. B., Delapp, D. M., Tokar, R. L., Young, D. T., Crary, F. J., et al. (2010). Survey of ion plasma parameters in Saturn's magnetosphere. *Journal of Geophysical Research*, *115*(A10), A10220. https://doi.org/10.1029/2010JA015267

Toledo-Redondo, S., Lee, J. H., Vines, S. K., Turner, D. L., Allen, R. C., Andre, M., et al. (2021). Kinetic interaction of cold and hot protons with an oblique EMIC wave near the dayside reconnecting magnetopause. *Geophysical Research Letters*, *48*(8), e2021GL092376. https://doi.org/10.1029/2021GL092376

Tsurutani, B. T. (1991). Comets: A laboratory for plasma waves and instabilities. In A. Johnstone (Ed.), *Cometary plasma processes* (Vol. *61*, 189–209). https://doi.org/10.1029/GM061p0189

Tsurutani, B. T., Chen, R., Gao, X., Lu, Q., Pickett, J. S., Lakhina, G. S., et al. (2020). Lower-band "monochromatic" chorus riser subelement/wave packet observations. *Journal of Geophysical Research: Space Physics*, *125*(10), e2020JA028090. https://doi.org/10.1029/2020JA028090

Tsurutani, B. T., & Smith, E. J. (1974). Postmidnight chorus: A substorm phenomenon. *Journal of Geophysical Research*, *79*(1), 118–127. https://doi.org/10.1029/JA079i001p00118

Tsurutani, B. T., Verkhoglyadova, O. P., Lakhina, G. S., & Yagitani, S. (2009). Properties of dayside outer zone chorus during HILDCAA events: Loss of energetic electrons. *Journal of Geophysical Research*, *114*(A3), A03207. https://doi.org/10.1029/2008JA013353

Usanova, M., Malaspina, D., Jaynes, A., Bruder, R., Mann, I., Wygant, J. R., & Ergun, R. (2016). Van Allen probes observations of oxygen cyclotron harmonic waves in the inner magnetosphere. *Geophysical Research Letters*, *43*(17), 8827–8834. https://doi.org/10.1002/2016GL070233

Usanova, M. E. (2021). Energy exchange between electromagnetic ion cyclotron (EMIC) waves and thermal plasma: From theory to observations. *Frontiers in Astronomy and Space Sciences*, *17*. https://doi.org/10.3389/fspas.2021.744344

Usanova, M. E., Ahmadi, N., Malaspina, D. M., Ergun, R. E., Trattner, K. J., Reece, Q., et al. (2018). MMS observations of harmonic electromagnetic ion cyclotron waves. *Geophysical Research Letters*, *45*(17), 8764–8772. https://doi.org/10.1029/2018GL079006

Vines, S. K., Allen, R. C., Anderson, B. J., Engebretson, M. J., Fuselier, S. A., Russell, C. T., et al. (2019). EMIC waves in the outer magnetosphere: Observations of an off-equator source region. *Geophysical Research Letters*, *46*(11), 5707–5716. https://doi.org/10.1029/2019GL082152

Vines, S. K., Anderson, B. J., Allen, R. C., Denton, R. E., Engebretson, M. J., Johnson, J. R., et al. (2021). Determining EMIC wave vector properties through multi-point measurements: The wave curl analysis. *Journal of Geophysical Research: Space Physics*, *126*(4), e2020JA028922. https://doi.org/10.1029/2020JA028922

Wolfram, S. (1988). *Mathematica: A system for doing mathematics by computer*. Adison-Wesley Publishing Company, Inc.

Young, D. T., Perraut, S., Roux, A., de Villedary, C., Gendrin, R., Korth, A., et al. (1981). Wave-particle interactions near Ω_{He+} observed on GEOS 1 and 2 1. Propagation of ion cyclotron waves in He$^+$-rich plasma. *Journal of Geophysical Research*, *86*(A8), 6755–6772. https://doi.org/10.1029/JA086iA08p06755

Yu, X. D., Yuan, Z. G., Wang, D. D., Huang, S. Y., Li, H. M., Yu, T., & Qiao, Z. (2017). Oxygen cyclotron harmonic waves observed using Van Allen Probes. *Science China Earth Sciences*, *60*(7), 1310–1316. https://doi.org/10.1007/s11430-016-9024-3

Zhang, J., Coffey, V. N., Chandler, M. O., Boardsen, S. A., Saikin, A. A., Mello, E. M., et al. (2017). Properties, propagation, and excitation of EMIC waves observed by MMS: A case study. *NASA-Final Report*.

Zhang, X.-J., Li, W., Thorne, R. M., Angelopoulos, V., Bortnik, J., Kletzing, C. A., et al. (2016). Statistical distribution of EMIC wave spectra: Observations from Van Allen Probes. *Geophysical Research Letters*, *43*(24). https://doi.org/10.1002/2016GL071158

Zhang, Y., Matsumoto, H., & Kojima, H. (1998). Lion roars in the magnetosheath: Geotail observations. *Journal of Geophysical Research*, *103*(A3), 4615–4626. https://doi.org/10.1029/97JA02519

Zhu, H., & Chen, L. (2019). On the observation of electrostatic harmonics associated with EMIC waves. *Geophysical Research Letters*, *46*(24), 14274–14281. https://doi.org/10.1029/2019GL085528